neocortex of AD patients than normal individuals [22]. There are several drawbacks to the use of this tracer, including its relatively low affinity to AD brain tissue ($K_d = 25$ nM) compared to PIB [23] and its slower clearance from the white matter region due to its higher lipophilicity (Log$P = 1.75$),[22] resulting in lower signal to background ratio than PIB–PET. However, the voxel-based analysis of BF-227–PET images indicated a pattern of tracer distribution distinct from that of PIB–PET.[12] Intriguingly, the preferential [^{11}C]BF-227 retention in the posterior neocortical region of the AD brain corresponded with an area containing a high density of neuritic plaques [4,22]. A preliminary report of the direct comparison of PIB–PET and BF-227–PET in the same AD patients additionally demonstrated a difference in the regional distribution of these two agents, which presumably reflects their different preference for various conformations of Aβ in the senile plaque generation process [24]. From these findings, we speculate that BF-227 detects neuritic plaques containing dense amyloid fibrils preferentially, compared to PIB–PET, and provides unique information about the Aβ pathology in AD patients. The early detection of Aβ deposition is important to begin medication to prevent a cognitive decline in the stage of MCI, since it appears that the deposition of Aβ starts earlier than the clinical diagnosis of dementia [25–27]. Approximately 20–30% of healthy, age-matched subjects exhibited neocortical retention of PIB, predominantly in the prefrontal and posterior cingulate cortices [15,16]. The demonstration of PIB retention in a proportion of normal individuals supports postmortem observations that Aβ aggregation predominantly occurs before the onset of dementia. However, there is currently no evidence that all PIB-positive normal individuals are destined to develop dementia. Highly sensitive detection of Aβ leads to a potential risk for misjudging the process of normal physiological aging as a pathological indicator of AD. The accurate prediction of AD progression is thus necessary to prevent the administration of non-essential treatments to individuals who are not at risk of converting to AD. In particular, a shift of brain Aβ from the soluble to fibrillar form is closely associated with onset of AD [28]. Thus, selective detection of dense amyloid fibrils would be advantageous to differentiate normal aging process from AD with high specificity, as the deposition of neuritic plaques is strongly associated with the earliest symptoms of AD [25]. Based on this background evidence, we anticipated that BF-227–PET would more accurately predict the conversion from MCI to AD than other imaging techniques.

Cognitive decline is reported to strongly correlate with cortical atrophy in AD, suggesting that cortical degeneration is the primary basis of cognitive decline in AD [5]. Thus, an increased rate of cerebral atrophy, as evaluated using MRI, is a diagnostic feature of AD that correlates with the clinical stage/severity and is thought to represent the macroscopic consequences of neuronal destruction [29–31]. Medial temporal lobe atrophy, as seen in MRI scans of AD patients, is a sensitive marker of AD even in its earliest stages. Volumetric analysis of the entorhinal cortex distinguished subjects who were destined to develop dementia from normal controls with high accuracy [32]. However, this approach is time-consuming and highly dependent on analyst expertise because it requires accurate manual outlining of the region of interest for the measurement. Voxel-based morphometry (VBM) has emerged as an ideal tool to visualize the changes in gray matter density in disease states. This technique has been reported to detect gray matter loss in MCI and AD patients. In addition, lower gray matter density has been reported in MCI converters compared with MCI non-converters [33–37]. These findings suggest that measurement of gray matter loss in the medial temporal lobe or the other regions might predict progression from MCI to AD with high accuracy. A direct comparison of MRI with PIB–PET was previously performed in the control, MCI and AD populations [38]. The distributions of hippocampal volume did not overlap between AD and normal control groups with the exception of one control subject, and MCI subjects are evenly distributed between the AD and normal controls. In contrast, PIB–PET uptake showed a bimodal distribution. While all AD subjects are tightly clustered in the high PIB retention range, both the normal control and MCI subjects segregate themselves into high and low PIB retention groups. The voxel-by-voxel comparisons of AD versus control patients revealed differences in the topographical distribution of amyloid deposition and in grey matter loss, suggesting that these two imaging strategies provide complementary information about AD pathology.

In this study, we performed amyloid-imaging PET using [^{11}C]BF-227 and VBM analysis of MRI images in subjects with MCI and AD. We investigated whether changes in BF-227 uptake and gray matter density were associated with later conversion to AD in MCI populations. Moreover, we examined the association of these measurements with cognitive function in AD and MCI converters to investigate whether these imaging strategies can track the severity of AD pathology.

2. Materials and methods

2.1. Staining of senile plaques using BF-227

Postmortem brain tissue from a 69-year-old male with autopsy-confirmed AD was obtained from Fukushimura Hospital (Toyohashi, Japan). Experiments were performed under the regulations of the hospital ethics committee. Serial sections (6 μm) taken from paraffin-embedded blocks of the temporal cortex were prepared in xylene and ethanol. Before BF-227 staining, quenching of autofluorescence was performed. The quenched tissue section was immersed in 100 μM of BF-227 containing 50% ethanol for 10 min. The section stained with BF-227 was then dipped briefly into water and rinsed in PBS for 60 min before coverslipping with FluorSave Reagent (Calbiochem, La Jolla, CA), and examined using an Eclipse E800 microscope (Nikon, Tokyo, Japan) equipped with a V-2A filter set (excitation 380–420 nm, dichroic mirror 430 nm, long pass filter 450 nm). An adjacent section was immunostained using a monoclonal antibody (mAb) against Aβ (6F/3D; Dako A/S, Glostrup, Denmark). After pretreatment with 90% formic acid for 5 min, sections were immersed in blocking solution for 30 min and then incubated for 60 min at 37 °C with 6F/3D at a dilution of 1:50. After incubation, sections were processed with the avidin–biotin method using a Pathostain ABC-POD(M) Kit (Wako, Osaka, Japan) and diaminobenzidine tetrahydrochloride.

2.2. Subjects

Patients recruited in the present study included 12 normal age-matched controls, 13 subjects with amnestic MCI, and 15 patients with AD. Diagnoses of probable AD were based on criteria from the National Institute of Neurological and Communicative Disorders and Stroke and the Alzheimer's Disease Related Disorders Association (NINCDS-ADRDA) [39]. The diagnosis of amnestic MCI was made according to the published criteria described previously [40]. All MCI subjects underwent medical and neuropsychological reevaluation at approximately 3 month intervals. Conversion to AD was diagnosed when (1) signs of deterioration of the general cognitive function were present and continued for at least 6 months, and (2) the patient's score on the Clinical Dementia Rating changed by more than 0.5 points. The MCI subjects were divided into two groups, MCI converters ($n = 6$) and MCI non-converters ($n = 7$). The MCI converters were defined as patients who eventually developed AD within a mean follow-up of 27.0 ± 7.9 months (range 14–30 months). The MCI non-converters were defined as having a transient memory loss or remaining cognitively stable through at least a 2 year follow-up (27.7 ± 2.2 months; range 25–30 months). The control group was recruited from volunteers who were not taking centrally-acting medications, had no cognitive impairment and had no cerebrovascular lesions identified via MRI. All subjects were screened using a questionnaire and medical history, and subjects with medical conditions potentially affecting the central nervous system were excluded. In addition, none

Please cite this article as: Waragai M, et al, Comparison study of amyloid PET and voxel-based morphometry analysis in mild cognitive impairment and Alzheimer's disease, J Neurol Sci (2009), doi:10.1016/j.jns.2009.06.005

Table 1
Demographic characteristics of the subjects.

	Control	MCI non-converter	MCI converter	AD
N	12	7	6	15
Age (year)	67.3 ± 2.7	77.6 ± 3.1	80.2 ± 4.1	71.0 ± 5.1
Gender (F/M)	6/6	2/5	4/2	8/7
MMSE	29.9 ± 0.3	26.3 ± 1.1	25.7 ± 2.0	19.8 ± 3.5

of the subjects had asymptomatic cerebral infarction detected via T2-weighted MRI. Demographic data for the subjects are shown in Table 1. Although the MCI converters and non-converters were statistically older than the control subjects and the AD patients, no statistical difference in age was observed between the MCI converters and the non-converters. The AD patients showed a significantly lower MMSE score than the MCI converters, non-converters, and control subjects ($p<0.05$), however, no statistical difference in MMSE score was observed between the MCI converters and the non-converters. The Committee on Clinical Investigation at Tohoku University School of Medicine and the Advisory Committee on Radioactive Substances at Tohoku University approved the study protocol.

3. MRI methods

All subjects underwent MRI with a 1.5 T MR scanner (GE Signa Hispeed, Milwaukee, WI). A three-dimensional volumetric acquisition of a T1-weighted gradient echo sequence produced a gapless series of thin axial sections using a vascular TOF SPGR sequence (echo time/repetition time, 2.4/50 ms; flip angle, 45°; acquisition matrix, 256×256; 1 excitation; field of view, 22 cm; slice thickness, 2.0 mm). Cerebral atrophy was evaluated by VBM [41]. For spatial normalization, a 12-parameter affine transformation was used to avoid segmentation errors caused by the partial-volume effects inherently created by warping. The normalized MRI was then segmented into gray matter, white matter, cerebrospinal fluid, and other components using SPM2 or SPM5 software. The segmentation procedure involved calculating the Bayesian probability of each voxel belonging to each tissue class based on a priori MRI information with a non-uniformity correction. The segmented gray matter images were then subjected to affine and non-linear spatial normalization using a template of a priori gray matter. The spatially normalized gray matter images were smoothed with an isotropic Gaussian kernel (12 mm at full width at half maximum) using the partial-volume effects to create a spectrum of gray matter intensities. The resulting gray matter intensities were equivalent to the weighted average of gray matter voxels located in the volume fixed by the smoothing kernel. Regional intensities can thus be considered equivalent to gray matter concentration. Differences of gray matter intensities between groups were assessed using a *t*-test with a height threshold of $p<0.05$, corrected for multiple comparisons by the family-wise error method. The extent threshold was set to 100 voxels. Parahippocampal gray matter density was additionally evaluated by calculating the average intensities in the bilateral parahippocampal region of interest (ROI) using Dr.View/LINUX software (AJS, Japan). To evaluate global atrophy, a Z-score map was created via the comparison of individual gray matter images with the mean and S.D. of gray matter images of healthy controls after voxel normalization to global mean intensities. The degree of global atrophy (% global atrophy) was calculated as a ratio of the area in which the Z-score of the voxel was more than 2.0 to whole brain area, using Voxel-Based Specific Regional Analysis System for AD (VSRAD) software (Eisai, Tokyo, Japan) [42].

3.1. PET procedure

Radiosynthesis of [^{11}C]BF-227 and the procedure used for BF-227–PET were performed as described previously. [22] BF-227 and its N-desmethylated derivative (a precursor of [^{11}C]BF-227) were custom-synthesized by Tanabe R&D Service Co. [^{11}C]BF-227 was synthesized from its precursor by N-methylation in dimethyl sulfoxide using [^{11}C]methyl triflate. The [^{11}C]BF-227–PET study was performed using a PET SET-2400W scanner (Shimadzu Inc., Japan). After an intravenous injection of 211–366 mBq [^{11}C]BF-227, dynamic PET images were obtained for 60 min with the subject's eyes closed. Standardized uptake value (SUV) images of [^{11}C]BF-227 were obtained by normalizing the tissue radioactivity concentration to the injected dose and body weight. ROIs were placed on individual axial MR images in the cerebellar hemisphere and the frontal, lateral temporal, parietal and posterior cingulate cortices. The ROI information was then copied onto the dynamic PET SUV images, and regional SUVs were sampled using Dr.View/LINUX software. The ratio of the regional to cerebellar SUV (SUVR) at 40–60 min post-injection was calculated, and averaged SUVR values in the frontal, temporal, parietal and posterior cingulate cortices were considered representative of BF-227 retention in the neocortex (neocortical SUVR).

3.2. Statistical analysis

Statistical comparison of PET and MRI measurements in the four groups was performed via an analysis of variance followed by a Bonferroni multiple comparisons test with a significance level of $p<0.05$. Statistical comparisons of age and MMSE scores in the four groups were performed using a Kruskal–Wallis test followed by a Dunn's multiple comparison test with a significance level of $p<0.05$. Correlations between the MMSE score and BF-227 retention in the neocortex or the cerebral atrophy index were examined using a non-parametric Spearman's rank correlation analysis. Correlations between the brain atrophy index and BF-227 retention were determined using Pearson's correlations. A linear model was applied to the data to obtain a correlation coefficient and *p* value. These analyses were performed using GraphPad Prism5 software (GraphPad, San Diego, CA).

4. Results

In order to confirm the selective binding ability of BF-227 to Aβ deposits, neuropathological examination was initially performed using BF-227 staining of AD temporal brain sections. Senile plaques were selectively stained with BF-227 and the staining pattern coincided well with Aβ immunostaining in an adjacent section (Fig. 1). Strikingly, cored plaques were intensely stained with BF-227, indicating preferential BF-227 binding to dense Aβ fibrils. Next,

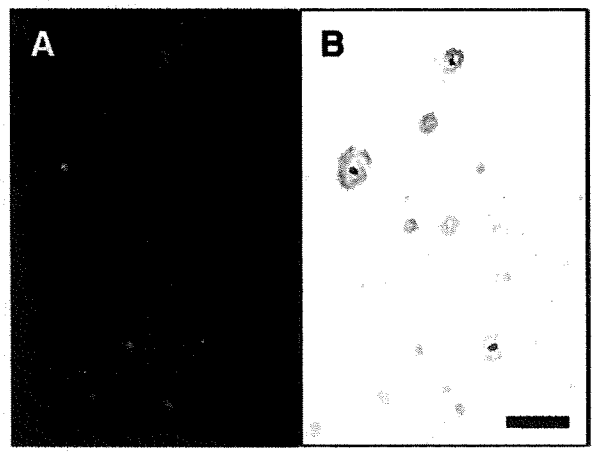

Fig. 1. (A) Neuropathological staining of human brain sections by BF-227. Amyloid plaques are clearly stained with BF-227 in AD temporal brain sections (B) BF-227 staining correlates well with Aβ immunostaining in adjacent sections. Scale bar = 100 μm.

Please cite this article as: Waragai M, et al, Comparison study of amyloid PET and voxel-based morphometry analysis in mild cognitive impairment and Alzheimer's disease, J Neurol Sci (2009), doi:10.1016/j.jns.2009.06.005

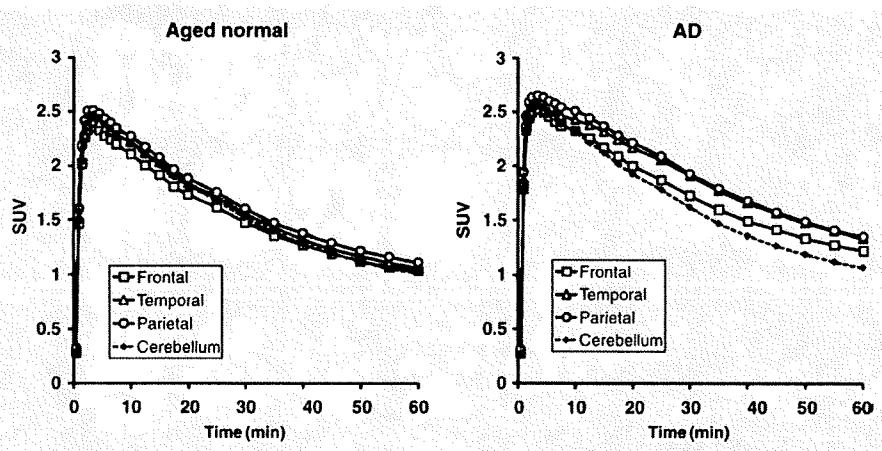

Fig. 2. Tissue time activity data for [^{11}C]BF-227–PET. SUV time activity curves of [^{11}C]BF-227 in the frontal cortex, lateral temporal cortex, parietal cortex and cerebellum are shown. Each point represents the mean of 12 control subjects (left) and 15 AD patients (right).

we performed clinical PET using [^{11}C]BF-227 in AD patients, MCI subjects and control subjects. The tissue time activity curves from [^{11}C]BF-227–PET in 15 AD patients and 12 normal controls are shown in Fig. 2. In AD patients, the frontal, temporal and parietal cortices retained [^{11}C]BF-227 to a greater extent at later time points, compared with controls. AD patients showed significantly higher SUVs in the temporal cortex and average neocortex than controls, but not in the cerebellum (Table 2). Therefore, neocortical SUV elevation in AD patients presumably reflects the specific binding of BF-227 to amyloid plaques. Representative images of [^{11}C]BF-227–PET and T1-weighted MRI in a normal control (70-year-old female, MMSE score 29), a MCI non-converter (76-year-old male, MMSE score 27), a MCI converter (85-year-old male, MMSE score 23), and an AD patient (62-year-old female, MMSE score 20) are shown in Fig. 3. Increased BF-227 retention was evident in both the MCI converter and the AD patient, but not in the control subject or the MCI non-converter. In AD patients, BF-227 SUVRs in the frontal, temporal, parietal and posterior cingulate cortices were significantly higher compared to the control subjects and the MCI non-converters (Table 2). A significant elevation of BF-227 SUVR was additionally observed in the frontal, temporal and parietal cortices of MCI converters compared with the control subjects. Consequently, the average neocortical SUVR was significantly higher in the AD patients and MCI converters than in normal subjects and MCI non-converters (Table 2). When a neocortical BF-227 SUVR of 1.11 (1.5SD above control mean) was used as a cut-off, sensitivity of 100% and a specificity of 91.7% in the discrimination between AD patients and normal subjects were achieved.

The voxel-based comparison of gray matter images using SPM5 demonstrated a significant decline of gray matter concentrations in the left ($-28, 14, -26, x, y, z$; $Z = 5.26$) and the right (32, 18, $-26, x, y, z$; $Z = 5.24$) medial temporal cortices of AD patients, compared with control subjects (Fig. 4A). SPM2 analysis using the same samples also showed a reduction of gray matter concentrations in nearly the same region and significance (data not shown). We drew the ROI in the parahippocampal area (Fig. 4B) and performed a comparison between the four groups. Significantly lower gray matter intensity was observed in the AD patients, MCI converters and MCI non-converters than in controls (Table 2, Fig. 5). However, age-related changes may be a confounding factor resulting in lower gray matter intensity in MCI groups, as MCI subjects were older than the normal control group. When a parahippocampal ROI value from SPM5 of 0.537 (2SD below control mean) was used as a cut-off, a sensitivity of 80.0% and a specificity of 100% were achieved in the discrimination between AD patients and normal subjects. No significant inter-group difference was observed in the percent global atrophy in VBM analysis due to substantial differences between individuals.

We focused on the comparison between the MCI converters and the non-converters, because these two populations showed no significant difference in age or MMSE scores. A significant inter-group difference was observed in the frontal and the average neocortical SUVR assayed by BF-227–PET, but not in the percent global atrophy or parahippocampal ROI value obtained by VBM–MRI (Table 2, Fig. 5). However, MCI converters showed a tendency toward lower parahippocampal ROI value derived from SPM5 than MCI non-converters.

Table 2
Summary of imaging measures.

	Normal	MCI non-converter	MCI converter	AD
BF-227 SUV in cerebellum	1.10 ± 0.19	1.08 ± 0.17	1.16 ± 0.22	1.16 ± 0.16
BF-227 SUV in frontal cortex	1.11 ± 0.19	1.10 ± 0.16	1.36 ± 0.33	1.31 ± 0.22
BF-227 SUV in temporal cortex	1.14 ± 0.19	1.19 ± 0.18	1.39 ± 0.28	1.45 ± 0.24[a]
BF-227 SUV in parietal cortex	1.20 ± 0.21	1.20 ± 0.18	1.38 ± 0.29	1.46 ± 0.23
BF-227 SUV in posterior cingulate cortex	1.22 ± 0.22	1.23 ± 0.22	1.39 ± 0.27	1.47 ± 0.21
Average neocortical BF-227 SUV	1.17 ± 0.20	1.18 ± 0.18	1.38 ± 0.29	1.42 ± 0.22[a]
BF-227 SUVR in frontal cortex	1.01 ± 0.06	1.02 ± 0.07	1.16 ± 0.10[a,b]	1.13 ± 0.08[a,b]
BF-227 SUVR in temporal cortex	1.04 ± 0.04	1.10 ± 0.07	1.20 ± 0.07[a]	1.24 ± 0.08[a,b]
BF-227 SUVR in parietal cortex	1.09 ± 0.04	1.12 ± 0.05	1.18 ± 0.07[a]	1.25 ± 0.08[a,b]
BF-227 SUVR in posterior cingulate cortex	1.11 ± 0.06	1.14 ± 0.07	1.20 ± 0.09	1.26 ± 0.05[a,b]
Average neocortical BF-227 SUVR	1.06 ± 0.04	1.09 ± 0.06	1.19 ± 0.07[a,b]	1.22 ± 0.06[a,b]
Percent global atrophy in VBM–MRI	4.24 ± 3.49	7.35 ± 5.94	5.96 ± 3.06	8.53 ± 4.44
Parahippocampal ROI value in VBM-MRI (SPM2)	0.642 ± 0.034	0.569 ± 0.039[a]	0.553 ± 0.044[a]	0.541 ± 0.055[a]
Parahippocampal ROI value in VBM-MRI (SPM5)	0.605 ± 0.034	0.510 ± 0.051[a]	0.473 ± 0.060[a]	0.475 ± 0.068[a]

[a] $p < 0.05$ vs. aged normal.
[b] $p < 0.05$ vs. MCI non-converter.

Please cite this article as: Waragai M, et al, Comparison study of amyloid PET and voxel-based morphometry analysis in mild cognitive impairment and Alzheimer's disease, J Neurol Sci (2009), doi:10.1016/j.jns.2009.06.005

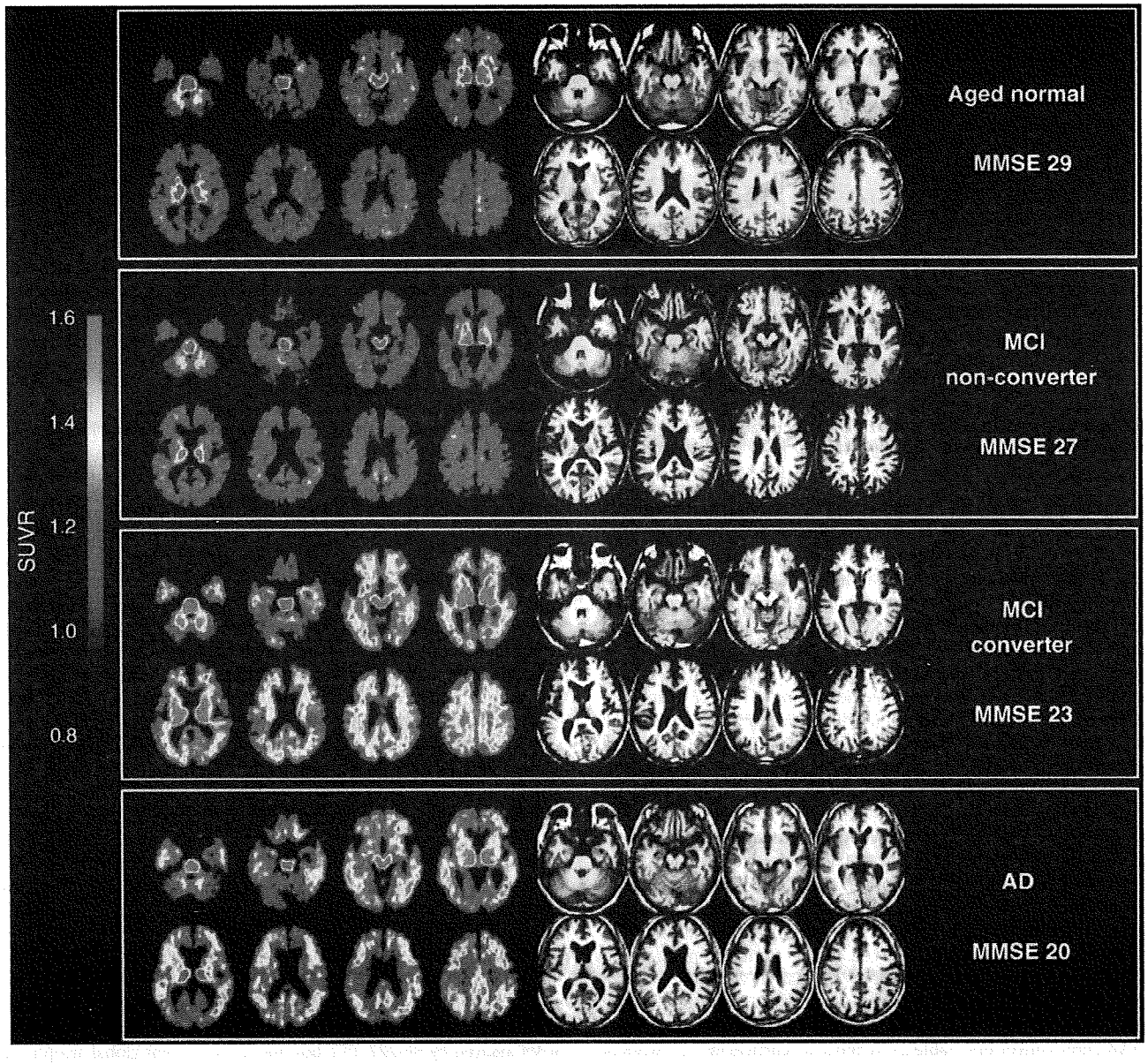

Fig. 3. Representative images of [^{11}C]BF-227-PET SUVR between 20 and 40 min post-injection (left) and T1-weighted MRI (right) in a control subject, a MCI non-converter, a MCI converter and an AD subject. The degree of [^{11}C]BF-227 retention is shown by color intensity from yellow to red in the cortex.

When we used a neocortical BF-227 SUVR of 1.11 as a cut-off, we achieved a sensitivity of 100% and a specificity of 71.4% in the discrimination between MCI converters and the MCI non-converters. These values were superior to the results of the parahippocampal ROI value derived from SPM5 (cut-off value: 0.537), which showed a sensitivity of 83.3% and a specificity of 42.9%. These data suggest that BF-227-PET is a better predictor of conversion from MCI to AD than VBM-MRI.

Next, we examined the correlations between MMSE scores and the three volume measurements (Fig. 6). When all subjects ($N=40$) were included in this analysis, a significant negative correlation was observed in all three measurements (BF-227 SUVR $r=-0.740$, $p<0.001$; percent global atrophy $r=-0.491$, $p=0.001$; parahippocampal ROI from SPM2 $r=0.674$, $p<0.001$; and parahippocampal ROI from SPM5 $r=0.687$, $p<0.001$). However, when we confined the analysis to the combined group of AD patients and MCI converters, we observed a significant correlation only between the percent global atrophy and the MMSE score (Spearman $r=-0.459$, $p=0.036$). In contrast, no significant correlation was observed between the parahippocampal ROI from SPM2 and the MMSE (Spearman $r=0.192$), between the parahippocampal ROI from SPM5 and the MMSE (Spearman $r=0.181$) or between the BF-227 SUVR in the neocortex and the MMSE (Spearman $r=-0.200$). Finally, no significant correlation was observed between the BF-227 SUVR and the percent global atrophy or parahippocampal atrophy in the analysis of all subjects.

5. Discussion

In the present study, MCI converters were more clearly distinguished from MCI non-converters by BF-227-PET than by VBM-MRI. The MCI non-converters showed a normal distribution of BF-227 except for one case, but also showed lower gray matter density in the parahippocampal gyrus than did normal controls. As a result, BF-227-PET achieved higher sensitivity and specificity in the discrimination between MCI converters and MCI non-converters than did VBM-MRI.

Please cite this article as: Waragai M, et al, Comparison study of amyloid PET and voxel-based morphometry analysis in mild cognitive impairment and Alzheimer's disease, J Neurol Sci (2009), doi:10.1016/j.jns.2009.06.005

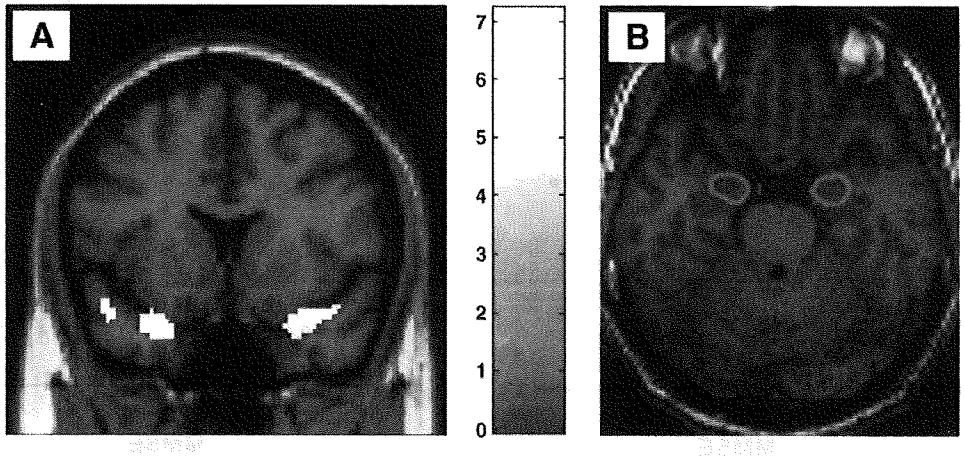

Fig. 4. (A) Areas of reduction in gray matter density of AD patients compared with aged normal controls. $p < 0.05$, corrected for multiple comparisons. Left in the image is left in the brain. Color bars represent T values. (B) Regions of interest within the parahippocampal gyrus.

Our results strongly suggest that amyloid imaging using BF-227–PET will be a useful tool to predict conversion from MCI to AD, as previously shown for PIB–PET. [17,18] However, cerebral gray matter loss as determined by VBM–MRI was better correlated with the clinical severity of AD than BF-227–PET. Used together, BF-227–PET and VBM–MRI could be an effective method for the early diagnosis and severity tracking of AD. Our findings may be compatible with the theory that amyloid deposition reaches equilibrium or plateaus at an early stage of AD, making in vivo amyloid imaging useful in the examination of pre-symptomatic subjects [15,16]. Aβ deposition is a pathological hallmark of AD, but may also occur in normal elderly individuals who do not exhibit apparent cognitive decline. In fact, a PIB–PET study showed that 22% of healthy elderly individuals showed increased cortical PIB binding, indicating the presence of Aβ plaques in these non-symptomatic subjects [15]. A strong relationship between the impairment of episodic memory and PIB binding has also been shown both in subjects with MCI and in the normal population, suggesting that individuals with increased cortical PIB

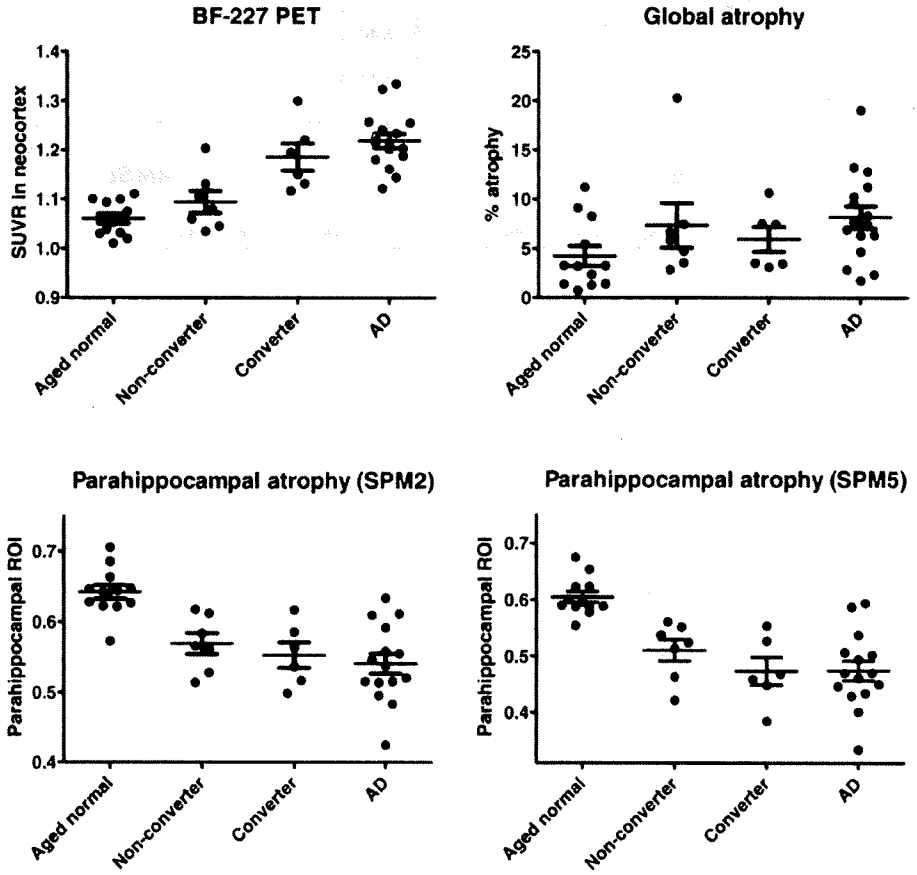

Fig. 5. Comparison of BF-227 SUVR in the neocortex (upper left), the percent global atrophy (upper right), the parahippocampal region of interest (ROI) value from gray matter images processed by SPM2 (lower left) and the parahippocampal ROI value from gray matter images processed by SPM5 (lower right) in control subjects, MCI non-converters, converters and AD patients.

Please cite this article as: Waragai M, et al, Comparison study of amyloid PET and voxel-based morphometry analysis in mild cognitive impairment and Alzheimer's disease, J Neurol Sci (2009), doi:10.1016/j.jns.2009.06.005

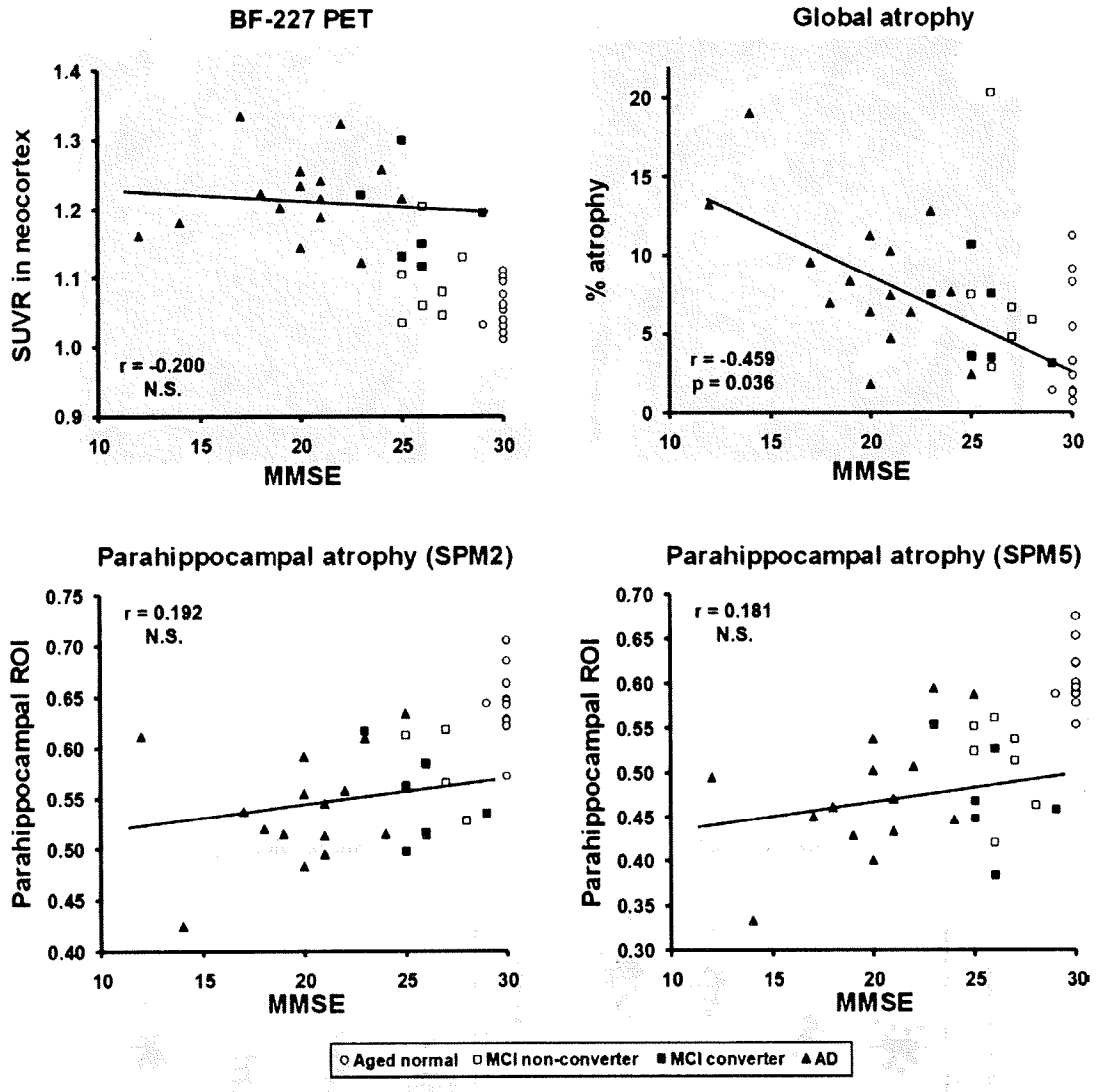

Fig. 6. The correlations of MMSE scores with the BF-227 SUVR in the neocortex (upper left), the percent global atrophy (upper right), the parahippocampal region of interest (ROI) value from gray matter images processed by SPM2 (lower left), and the parahippocampal ROI value from gray matter images processed by SPM5 (lower right). Open circle: control; open square: MCI non-converter; filled square: MCI converter; filled triangle: AD.

binding are proceeding to AD [43]. In our study, almost all normal subjects exhibited a normal distribution of BF-227 in the brain. This finding may suggest a lower sensitivity of diffuse amyloid plaque detection by BF-227 [22]. However, the proportion of amyloid PET-positive individuals in the normal population varies greatly depending on the characteristics of the sample population. Indeed, the mean age of the control subjects in our study was somewhat younger than in previous PIB–PET studies. Therefore, a direct comparison of BF-227–PET with PIB–PET in the same normal population is necessary to compare the ability of these agents to detect early AD pathology. A longitudinal follow-up of amyloid PET-positive cases in the healthy, normal population will also elucidate whether tracer uptake reflects pre-symptomatic detection of AD or a false-positive finding. A follow-up study of the patients with AD using PIB–PET showed that the amyloid deposition remains high but stable, despite decreases in regional glucose metabolism and cognitive function.[44] Our cross-sectional analysis also revealed a plateau of cortical BF-227 uptake in early AD patients, suggesting that amyloid formation reaches a plateau early in the course of AD. A potential limitation of this study is that it used a semiquantitative SUV measure to estimate BF-227 binding to amyloid plaques. The levels of neocortical BF-227 SUV might be underestimated due to hypoperfusion in AD patients. Quantitative analysis should be performed in future analyses to eliminate the influence of blood flow change.

A previous PIB–PET study found a positive correlation between the rate of whole brain atrophy and amyloid plaque load. [45] However, a recent PET study discovered a discrepancy between regional PIB retention and gray matter loss [38]. Additionally, histopathological analysis revealed no association between Aβ burden and brain atrophy [46]. The present study also found no significant correlation between neocortical BF-227 uptake and global gray matter loss in AD patients, in agreement with these findings. In our correlation analysis of the four measurements with the MMSE scores, we confined our analysis to AD patients and MCI converters because these patients share the same pathological process underlying AD. Therefore, this is more appropriate for the correlation analysis between cognitive function and the degree of Aβ burden or cerebral atrophy induced by the pathological process of AD than an analysis using all samples, including the normal population. In this analysis, the global gray matter loss measured by VBM–MRI was better correlated with MMSE scores than was the Aβ burden measured by BF-227–PET. A similar correlation analysis performed using PIB–PET demonstrated that the

Please cite this article as: Waragai M, et al, Comparison study of amyloid PET and voxel-based morphometry analysis in mild cognitive impairment and Alzheimer's disease, J Neurol Sci (2009), doi:10.1016/j.jns.2009.06.005

magnitudes of the correlations were greater for hippocampal atrophy than for neocortical PIB retention [38]. The current result, showing no significant correlation of the parahippocampal gray matter density with the MMSE score, seems to be inconsistent with previous PIB–PET data. We believe this discrepancy to be due mainly to differences in the sample population. The analysis in the previous PIB–PET study was performed using all the subjects, including the normal controls; our analysis was confined to AD patients and MCI converters who had already developed severe memory decline and probably substantial neuron loss in the hippocampus. These results suggest that global, rather than parahippocampal, gray matter loss is a potent indicator of dementia severity after the onset of memory loss in AD. We hope to explore the relationship between these imaging measurements and the impairment of episodic memory function in a future study.

It has been reported that the degree or rate of change of cerebral atrophy as measured by MRI analysis is closely related to the clinical progression of dementia [29,30]. Karas et al. performed a VBM–MRI analysis to examine the global and regional gray matter loss in normal, MCI and AD subjects, finding a significantly lower global gray matter volume in the AD subjects and an intermediate volume in the MCI subjects [31]. They followed the MCI subjects and observed greater gray matter loss in the MCI converters than in non-converters [37]. Another study also revealed different patterns of gray matter density distribution between MCI converters and non-converters [35]. From these findings, it appears that gray matter loss in VBM is a good indicator of conversion from MCI to AD. We failed to demonstrate significant inter-group differences between the MCI converters and non-converters, although the MCI converters showed a tendency toward lower parahippocampal gray matter density than did the non-converters. This, however, may be due to the small sample size and insufficient follow-up period (over two years) of the MCI subjects in this study. For example, one MCI non-converter in our study showed an abnormality in both the BF-227 SUVR and parahippocampal gray matter density; extending the follow-up period of the MCI subjects would likely result in more consistent correlation between MCI conversion to AD and the described measurements. Additional longitudinal studies are also needed to confirm the findings we have obtained and to examine the time course of AD, including changes in the pre-symptomatic subjects, and to determine the relationship between amyloid deposition and brain atrophy as underlying factors in the pathogenesis of AD.

Acknowledgements

We appreciate the technical assistance of Dr. S. Watanuki, Dr. Y. Ishikawa, Dr. M. Mori, and Dr. K. Sugi in the clinical PET studies and the support of Fukushimura Hospital for the histochemical studies. We also thank to Dr. H. Akatsu and Dr. T. Yamamoto for supplying brain samples. This study was supported by the Program for the Promotion of Fundamental Studies in Health Science of the National Institute of Biomedical Innovation, the Industrial Technology Research Grant Program in 2004 of the New Energy and Industrial Technology Development Organization (NEDO) of Japan, Health and Labor Sciences Research Grants for Translational Research from the Ministry of Health, an Asan Trazeneca Research Grant, and the Novartis Foundation for Gerontological Research.

References

[1] Blennow K, de Leon MJ, Zetterberg H. Alzheimer's disease. Lancet 2006;368: 387–403.
[2] Drachman DA. Aging of the brain, entropy, and Alzheimer disease. Neurology 2006;67:1340–52.
[3] Braak H, Braak E. Neuropathological stageing of Alzheimer-related changes. Acta Neuropathol 1991;82:239–59.
[4] Arnold SE, Hyman BT, Flory J, Damasio AR, Van Hoesen GW. The topographical and neuroanatomical distribution of neurofibrillary tangles and neuritic plaques in the cerebral cortex of patients with Alzheimer's disease. Cereb Cortex 1991;1:103–16.
[5] Mouton PR, Martin LJ, Calhoun ME, Dal Forno G, Price DL. Cognitive decline strongly correlates with cortical atrophy in Alzheimer's dementia. Neurobiol Aging 1998;19:371–7.
[6] Masters CL, Cappai R, Barnham KJ, Villemagne VL. Molecular mechanisms for Alzheimer's disease: implications for neuroimaging and therapeutics. J Neurochem 2006;97:1700–25.
[7] Nordberg A. PET imaging of amyloid in Alzheimer's disease. Lancet Neurol 2004;3: 519–27.
[8] Villemagne VL, Rowe CC, Macfarlane S, Novakovic KE, Masters CL. Imaginem oblivionis: the prospects of neuroimaging for early detection of Alzheimer's disease. J Clin Neurosci 2005;12:221–30.
[9] Mathis CA, Klunk WE, Price JC, DeKosky ST. Imaging technology for neurodegenerative diseases: progress toward detection of specific pathologies. Arch Neurol 2005;62:196–200.
[10] Nordberg A. Amyloid imaging in Alzheimer's disease. Curr Opin Neurol 2007;20: 398–402.
[11] Small GW, Kepe V, Ercoli LM, Siddarth P, Bookheimer SY, Miller KJ, et al. PET of brain amyloid and tau in mild cognitive impairment. N Engl J Med 2006;355:2652–63.
[12] Klunk WE, Engler H, Nordberg A, Wang Y, Blomqvist G, Holt DP, et al. Imaging brain amyloid in Alzheimer's disease with Pittsburgh Compound-B. Ann Neurol 2004;55:306–19.
[13] Price JC, Klunk WE, Lopresti BJ, Lu X, Hoge JA, Ziolko SK, et al. Kinetic modeling of amyloid binding in humans using PET imaging and Pittsburgh Compound-B. J Cereb Blood Flow Metab 2005;25:1528–47.
[14] Lopresti BJ, Klunk WE, Mathis CA, Hoge JA, Ziolko SK, Lu X, et al. Simplified quantification of Pittsburgh Compound B amyloid imaging PET studies: a comparative analysis. J Nucl Med 2005;46:1959–72.
[15] Rowe CC, Ng S, Ackermann U, Gong SJ, Pike K, Savage G, et al. Imaging beta-amyloid burden in aging and dementia. Neurology 2007;68:1718–25.
[16] Mintun MA, Larossa GN, Sheline YI, Dence CS, Lee SY, Mach RH, et al. [^{11}C]PIB in a nondemented population: potential antecedent marker of Alzheimer disease. Neurology 2006;67:446–52.
[17] Fripp J, Bourgeat P, Acosta O, Raniga P, Modat M, Pike KE, et al. Appearance modeling of ^{11}C PiB PET images: characterizing amyloid deposition in Alzheimer's disease, mild cognitive impairment and healthy aging. Neuroimage 2008;43:430–9.
[18] Forsberg A, Engler H, Almkvist O, Blomquist G, Hagman G, Wall A, et al. PET imaging of amyloid deposition in patients with mild cognitive impairment. Neurobiol Aging 2008;29:1456–65.
[19] Okamura N, Suemoto T, Shimadzu H, Suzuki M, Shiomitsu T, Akatsu H, et al. Styrylbenzoxazole derivatives for in vivo imaging of amyloid plaques in the brain. J Neurosci, 2004;24:2535–41.
[20] Okamura N, Furumoto S, Funaki Y, Suemoto T, Kato M, Ishikawa Y, et al. Binding and safety profile of novel benzoxazole derivative for in vivo imaging of amyloid deposits in Alzheimer's disease. Geriatr Gerontol Int 2007;7:393–400.
[21] Furumoto S, Okamura N, Iwata R, Yanai K, Arai H, Kudo Y. Recent advances in the development of amyloid imaging agents. Curr Top Med Chem 2007;7:1773–89.
[22] Kudo Y, Okamura N, Furumoto S, Tashiro M, Furukawa K, Maruyama M, et al. 2-(2-[2-Dimethylaminothiazol-5-yl]Ethenyl)-6-(2-[Fluoro]Ethoxy)Benzoxazole: A novel PET agent for in vivo detection of dense amyloid plaques in Alzheimer's disease patients. J Nucl Med 2007;48:553–61.
[23] Fodero-Tavoletti MT, Mulligan RS, Okamura N, Furumoto S, Rowe CC, Kudo Y, et al. In vitro characterization of BF227 binding to α-synuclein/Lewy Bodies. Eur J Pharmacol. (in press).
[24] Ishii K, Hashimoto M, Kimura Y, Sakata M, Oda K, Kawasaki K, et al. Direct comparison of in vivo accumulation of ^{11}C-PIB and ^{11}C-BF227 in Alzheimer's disease. Alzheimer's and Dementia, vol. 4, Issue 4; July 2008. p. T49. Supplement 1.
[25] Tiraboschi P, Hansen LA, Thal LJ, Corey-Bloom J. The importance of neuritic plaques and tangles to the development and evolution of AD. Neurology 2004;62:1984–9.
[26] Price JL, Morris JC. Tangles and plaques in nondemented aging and "preclinical" Alzheimer's disease. Ann Neurol 1999;45:358–68.
[27] Morris JC, Storandt M, Miller JP, McKeel DW, Price JL, Rubin EH, et al. Mild cognitive impairment represents early-stage Alzheimer disease. Arch Neurol 2001;58:397–405.
[28] Wang J, Dickson DW, Trojanowski JQ, Lee VM. The levels of soluble versus insoluble brain Abeta distinguish Alzheimer's disease from normal and pathologic aging. Exp Neurol 1999;158:328–37.
[29] Fox NC, Crum WR, Scahill RI, Stevens JM, Janssen JC, Rossor MN. Imaging of onset and progression of Alzheimer's disease with voxel-compression mapping of serial magnetic resonance images. Lancet 2001;358:201–5.
[30] Jack Jr CR, Shiung MM, Gunter JL, O'Brien PC, Weigand SD, Knopman DS, et al. Comparison of different MRI brain atrophy rate measures with clinical disease progression in AD. Neurology 2004;62:591–600.
[31] Karas GB, Scheltens P, Rombouts SA, Visser PJ, van Schijndel RA, Fox NC, et al. Global and local gray matter loss in mild cognitive impairment and Alzheimer's disease. Neuroimage 2004;23:708–16.
[32] Killiany RJ, Gomez-Isla T, Moss M, Kikinis R, Sandor T, Jolesz F, et al. Use of structural magnetic resonance imaging to predict who will get Alzheimer's disease. Ann Neurol 2000;47:430–9.
[33] Bell-McGinty S, Lopez OL, Meltzer CC, Scanlon JM, Whyte EM, Dekosky ST, et al. Differential cortical atrophy in subgroups of mild cognitive impairment. Arch Neurol 2005;62:1393–7.
[34] Chetelat G, Landeau B, Eustache F, Mezenge F, Viader F, de la Sayette V, et al. Using voxel-based morphometry to map the structural changes associated with rapid conversion in MCI: a longitudinal MRI study. Neuroimage 2005;27:934–46.
[35] Bozzali M, Filippi M, Magnani G, Cercignani M, Franceschi M, Schiatti E, et al. The contribution of voxel-based morphometry in staging patients with mild cognitive impairment. Neurology 2006;67:453–60.

Please cite this article as: Waragai M, et al, Comparison study of amyloid PET and voxel-based morphometry analysis in mild cognitive impairment and Alzheimer's disease, J Neurol Sci (2009), doi:10.1016/j.jns.2009.06.005

[36] Hämäläinen A, Tervo S, Grau-Olivares M, Niskanen E, Pennanen C, Huuskonen J, et al. Voxel-based morphometry to detect brain atrophy in progressive mild cognitive impairment. Neuroimage 2007;37:1122–31.
[37] Karas G, Sluimer J, Goekoop R, van der Flier W, Rombouts SA, Vrenken H, et al. Amnestic mild cognitive impairment: structural MR imaging findings predictive of conversion to Alzheimer disease. Am J Neuroradiol 2008;29:944–9.
[38] Jack Jr CR, Lowe VJ, Senjem ML, Weigand SD, Kemp BJ, Shiung MM, et al. ^{11}C PiB and structural MRI provide complementary information in imaging of Alzheimer's disease and amnestic mild cognitive impairment. Brain 2008;131:665–80.
[39] McKhann G, Drachman D, Folstein M, Katzman R, Price D, Stadlan EM. Clinical diagnosis of Alzheimer's disease: report of the NINCDS-ADRDA Work Group under the auspices of Department of Health and Human Services Task Force on Alzheimer's Disease. Neurology 1984;34:939–44.
[40] Petersen RC, Smith GE, Waring SC, Ivnik RJ, Tangalos EG, Kokmen E. Mild cognitive impairment: clinical characterization and outcome. Arch Neurol 1999;56:303–8.
[41] Ashburner J, Friston KJ. Voxel-based morphometry—the methods. Neuroimage 2000;11:805–21.
[42] Hirata Y, Matsuda H, Nemoto K, Ohnishi T, Hirao K, Yamashita F, et al. Voxel-based morphometry to discriminate early Alzheimer's disease from controls. Neurosci Lett 2005;382:269–74.
[43] Pike KE, Savage G, Villemagne VL, Ng S, Moss SA, Maruff P, et al. Beta-amyloid imaging and memory in non-demented individuals: evidence for preclinical Alzheimer's disease. Brain 2007;130:2837–44.
[44] Engler H, Forsberg A, Almkvist O, Blomquist G, Larsson E, Savitcheva I, et al. Two-year follow-up of amyloid deposition in patients with Alzheimer's disease. Brain 2006;129:2856–66.
[45] Archer HA, Edison P, Brooks DJ, Barnes J, Frost C, Yeatman T, et al. Amyloid load and cerebral atrophy in Alzheimer's disease: an ^{11}C-PIB positron emission tomography study. Ann Neurol 2006;60:145–7.
[46] Josephs KA, Whitwell JL, Ahmed Z, Shiung MM, Weigand SD, Knopman DS, et al. Beta-amyloid burden is not associated with rates of brain atrophy. Ann Neurol 2008;63:204–12.

Please cite this article as: Waragai M, et al, Comparison study of amyloid PET and voxel-based morphometry analysis in mild cognitive impairment and Alzheimer's disease, J Neurol Sci (2009), doi:10.1016/j.jns.2009.06.005

NeuroImage 46 (2009) 616–623

Contents lists available at ScienceDirect

NeuroImage

journal homepage: www.elsevier.com/locate/ynimg

Quantitative analysis of donepezil binding to acetylcholinesterase using positron emission tomography and [5-^{11}C-*methoxy*]donepezil

Kotaro Hiraoka [a,*], Nobuyuki Okamura [b], Yoshihito Funaki [c], Shoichi Watanuki [d], Manabu Tashiro [d], Motohisa Kato [b], Akiko Hayashi [a], Yoshiyuki Hosokai [a], Hiroshi Yamasaki [a], Toshikatsu Fujii [a], Etsuro Mori [a], Kazuhiko Yanai [b], Hiroshi Watabe [e]

[a] Department of Behavioral Neurology and Cognitive Neuroscience, Tohoku University Graduate School of Medicine, 2-1, Seiryo-machi, Aoba-ku, Sendai, 980-8575, Japan
[b] Department of Pharmacology, Tohoku University Graduate School of Medicine, Sendai, Japan
[c] Division of Radiopharmaceutical Chemistry, Cyclotron and Radioisotope Center, Tohoku University, Sendai, Japan
[d] Division of Cyclotron Nuclear Medicine, Cyclotron and Radioisotope Center, Tohoku University, Sendai, Japan
[e] Department of Investigative Radiology, National Cardiovascular Center Research Institute, Osaka, Japan

ARTICLE INFO

Article history:
Received 17 September 2008
Revised 24 February 2009
Accepted 4 March 2009
Available online 12 March 2009

Keywords:
Acetylcholinesterase
Acetylcholinesterase inhibitor
Donepezil
Positron emission tomography (PET)

ABSTRACT

The aim of this study was to establish kinetic analysis of [5-^{11}C-*methoxy*]donepezil ([^{11}C]donepezil), which was developed for the in-vivo visualization of donepezil binding to acetylcholinesterase (AChE) using positron emission tomography (PET). Donepezil is an AChE inhibitor that is widely prescribed to ameliorate the cognitive impairment of patients with dementia. Six healthy subjects took part in a dynamic study involving a 60-min PET scan after intravenous injection of [^{11}C]donepezil. The total distribution volume (tDV) of [^{11}C]donepezil was quantified by compartmental kinetic analysis and Logan graphical analysis. A one-tissue compartment model (1TCM) and a two-tissue compartment model (2TCM) were applied in the kinetic analysis. Goodness of fit was assessed with χ^2 criterion and Akaike's Information Criterion (AIC). Compared with a 1TCM, goodness of fit was significantly improved by a 2TCM. The tDVs provided by Logan graphical analysis were slightly lower than those provided by a 2TCM. The rank order of the mean tDVs in 10 regions was in line with the AChE activity reported in a previous post-mortem study. Logan graphical analysis generated voxel-wise images of tDV, revealing the overall distribution pattern of AChE in individual brains. Significant correlation was observed between tDVs calculated with and without metabolite correction for plasma time–activity curves, indicating that metabolite correction could be omitted. In conclusion, this method enables quantitative analysis of AChE and direct investigation of the pharmacokinetics of donepezil in the human brain.

Introduction

The cholinergic system is one of the most crucial neurotransmitter systems in the brain, and it has very profound links with the manifestations of dementia (Francis et al., 1999; Perry et al., 1999). The activities of both choline acetyltransferase (ChAT), the enzyme catalyzing acetylcholine synthesis, and acetylcholinesterase (AChE), the enzyme degrading brain acetylcholine, are reported to be decreased in the neocortex and hippocampus of patients with Alzheimer's disease (AD) and Parkinson's disease with dementia (PDD) (Davies and Maloney, 1976; Perry et al., 1985), and this decreased activity correlates with the severity of cognitive impairment (Perry et al., 1978). Significant loss of cholinergic neurons in the nucleus basalis of Meynert has been reported in the brains of patients with both diseases (Whitehouse et al., 1982, 1983). Based on these pathological findings, the use of reversible AChEs was proposed as a means of potentiating cholinergic neurotransmission, with the aim of improving cognitive function.

Currently, several AChE inhibitors (AChEIs) are prescribed to improve the cognitive function of patients with dementia. Donepezil hydrochloride is an AChEI that has been proved to be effective in ameliorating the cognitive impairment of patients with AD (Rogers et al., 1998), and it is widely prescribed for the treatment of this disease.

Various radiotracers have been developed to visualize different types of neurotransmissions in the human brain using positron emission tomography (PET) (Lammertsma et al., 1991; Frey et al., 1996; Parsey et al., 2000; Sakata et al., 2007). These techniques for mapping receptors in the human brain have also provided the opportunity for the development of new drugs, for the evaluation of the therapeutic effects of the drugs, and for better decisions to be made about the appropriate doses of drugs for neurological and psychiatric diseases.

* Corresponding author. Fax: +81 22 717 7360.
E-mail address: khiraoka@mail.tains.tohoku.ac.jp (K. Hiraoka).

1053-8119/$ – see front matter © 2009 Elsevier Inc. All rights reserved.
doi:10.1016/j.neuroimage.2009.03.006

Some radiolabeled AChEIs such as [^{11}C]physostigmine and [^{11}C] methyl-tacrine, a tacrine derivative, have been synthesized for AChE imaging. Unfortunately, the kinetics of [^{11}C]physostigmine proved to be too complex, such that the required model was overspecified (Blomqvist et al., 2001). Amongst the other candidate AChE ligands tested, the distribution of [^{11}C]methyl-tacrine was not correlated with AChE activity in the brain of the baboon (Tavitian et al., 1993), and [6-^{11}C-*methoxy*]donepezil, which was also synthesized, was devoid of specific binding to AChE in vivo (De Vos et al., 2000).

[5-^{11}C-*methoxy*]donepezil ([^{11}C]donepezil) was originally developed by Funaki and coworkers (Funaki et al., 2003). The binding of [^{11}C]donepezil to homogenates of rat brain was highest in the brainstem and striatum, and lowest in the cerebellum, and in-vitro autoradiographic studies demonstrated specific binding to AChE. The 50% inhibitory concentration (IC_{50}) value of binding was about 10 nM, which is consistent with the reported value of inhibiting enzyme activity (6 nM). Saturation experiments showed that the maximum binding capacity (B_{max}) was 65 fmol/mg tissue, and the dissociation constant (K_d) of [^{11}C]donepezil binding was 39.8 nM in vitro. In-vivo distribution of [^{11}C]donepezil in rat brain was heterogeneous, in accordance with in-vitro binding. The blocking experiment in the earlier study by Funaki et al. showed that the heterogeneous pattern of binding seen in the baseline condition was considerably attenuated by co-injection of a large amount of unlabeled donepezil. In addition, a study by Okamura et al. (2008) revealed reduced binding of [^{11}C] donepezil in the brain of patients with AD, although this study was limited by use of the Logan graphical analysis method without fulfillment of the necessary criteria. However, these reports show that [^{11}C]donepezil holds promise as a potential agent for imaging AChE in vivo using PET.

The aim of this study was to establish a quantitative method of evaluating the binding of [^{11}C]donepezil to AChE in the human brain. We performed [^{11}C]donepezil-PET in six healthy subjects. First, a method for full-compartment analysis was investigated. Then, graphical analysis using the Logan plot (Logan et al., 1990) was applied to the data to visualize the spatial distribution of the binding parameter of [^{11}C]donepezil with AChE. The possibility of omitting metabolite correction for the plasma input function was also investigated as a convenient method of applying [^{11}C]donepezil-PET to various clinical situations.

Materials and methods

Subjects

Six elderly normal volunteers (four men and two women, mean age 65.8 ± 5.4 years) were recruited. The subjects had no cognitive impairment, no neurological disorders, and no abnormalities apparent on magnetic resonance images (MRIs) of their brains. None of them was receiving any centrally acting medication. All subjects underwent a PET scan with [^{11}C]donepezil. The Ethics Committee of Tohoku University School of Medicine approved the study protocol, and written informed consent was given by all subjects.

Radiosynthesis of [^{11}C]donepezil

[^{11}C]donepezil was synthesized (Fig. 1) as previously described (Funaki et al., 2003). Briefly, tetrabutylammonium hydroxide was added to 5′-O-demethylprecursor (M2), which was dissolved in methylethylketone. [^{11}C]methyliodide was produced from [^{11}C]CO_2 and converted to [^{11}C]methyl-triflate ([^{11}C]MeOTf). [^{11}C]donepezil was produced on the loop from [^{11}C]MeOTf and purified by preparative high-performance liquid chromatography (HPLC). The radioactivity of [^{11}C]donepezil was 155.4–814 MBq (4.2–22 mCi), and the radiochemical yield was estimated to be 25–30% based on [^{11}C] MeOTf after decay-correction. The specific activity of [^{11}C]donepezil at the end of synthesis was 111–354 GBq μmol^{-1}. Radiochemical purity was above 99%. The injected doses (mean ± standard deviation (SD)) were 210 ± 120 MBq (5.6 ± 3.2 mCi).

PET scan protocol

The PET scanner used was a SET-2400W (Shimadzu Co., Kyoto, Japan). This scanner acquires 63 image slices at a center-to-center interval of 3.125 mm and has a spatial resolution of 3.9 mm full width at half maximum (FWHM) and a Z-axis resolution of 6.5 FWHM at center of field of view (Fujiwara et al., 1997). The 7-min transmission data were acquired with a rotating [^{68}Ge]/[^{68}Ga] line source to correct for attenuation. Then, [^{11}C]donepezil was injected intravenously into each subject and a 60-min dynamic scan in 3D mode (30 s × 5 frames, 60 s × 5 frames, 150 s × 5 frames, 300 s × 8 frames) was performed.

Blood sampling and metabolite analysis

Arterial blood samples (2.5 mL) were collected from each patient's radial artery at 10-second intervals for the first 2 min, and subsequently at intervals increasing progressively from 1 to 10 min until 60 min after the injection of [^{11}C]donepezil. Each blood volume sample was 2.5 mL. To analyze the labeled metabolites, 8 mL of additional blood was obtained at 5, 15, and 30 min. The plasma obtained by centrifugation was weighed and the radioactivity was measured with a well-type scintillation counter, the sensitivity of which was calibrated with the PET scanner. Thus, the time–activity curve for arterial plasma (pTAC) was calculated as μCuries per millilitre (μCi/mL). The metabolites of [^{11}C]donepezil in the selected extra plasma samples were analyzed by HPLC. Briefly, sampled plasma

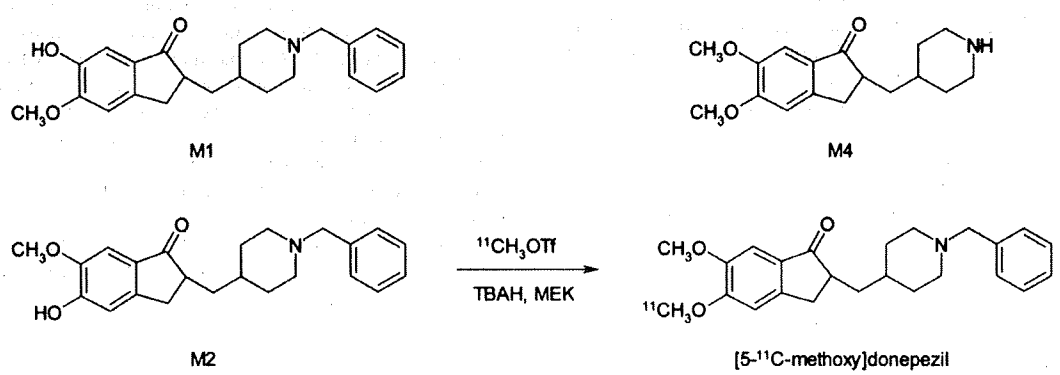

Fig. 1. Chemical structures of [5-^{11}C-*methoxy*]donepezil and donepezil metabolites. [5-^{11}C-*methoxy*]donepezil is synthesized from 5′-O-demethylprecursor (M2).

(4 mL) was treated with 1 M HCl_4:MeCN (7:3). After centrifugation at 3000 ×*g* for 3 min, the supernatant solution was injected into a semi-preparative HPLC column (YMC ODS A-324, YMC Co. Ltd., Kyoto, Japan; 10 mm i.d.× 30 cm long) with a solvent system of 0.1 M ammonium formate:acetonitrile (60:40) at a flow rate of 5.0 mL min^{-1}. The eluates were collected at 0.5-min intervals, and radioactivity was counted with a gamma-counter.

Metabolite correction was performed on pTAC values in subsequent data analyses. For this correction, the empirical function proposed by Watabe et al. for expressing the fraction of un-transformed tracer remaining at time *t* (Watabe et al., 2000), $1/(1+(\alpha t)^2)^{\beta}$ was fitted with a Nelder–Meads simplex algorithm (Nelder and Mead, 1965) using a least-squares method with initial guesses of 0.1 for both α and β.

PET image processing

Dynamic images were reconstructed with a 3D projection algorithm using a Butterworth–Cholsher filter with a cut-off frequency of 1.25 cycles/cm. The image matrix size was 128 × 128 × 63 voxels, and voxel size was 2 × 2 × 3.125 mm. PET images were co-registered with MRI using SPM5 (http://www.fil.ion.ucl.ac.uk/spm/software/spm5/). Multiple circular regions of interest (ROIs, 1.0 cm in diameter) were located on each region of brain, i.e., the frontal, temporal, parietal, and occipital cortices, hippocampus, putamen, thalamus, anterior and posterior cingulate gyrus, and cerebellar hemisphere. The volumes of the ROIs were between 2.88 cm^3 and 11.96 cm^3 (mean ± SD = 6.40 ± 2.50 cm^3). Time–activity curves in the tissues (tTACs) were calculated as μCuries per millilitre.

Kinetic analysis

For kinetic analysis, one-tissue compartment (1TCM) and two-tissue compartment (2TCM) models were applied. In the latter, based on the assumption that the non-specific binding component is in equilibrium with a free component (Koeppe et al., 1991), compartment models were fitted on the tTAC. The composition and relation of the compartments in 1TCM and 2TCM are shown in Fig. 2. In the 1TCM, C_p and C_t denote the concentration of radioligand in arterial plasma and the tissue compartment, respectively. K_1 describes transfer from plasma to tissue through the blood–brain barrier (BBB), and k_2 denotes a rate constant of back-diffusion from tissue to plasma. In the 2TCM, C_p, C_f, and C_b represent the concentration of radioligand in arterial plasma, the free compartment, and the specifically bound compartment, respectively; K_1 describes transfer from plasma to tissue through the BBB, and k_2 represents a rate constant of back-diffusion from tissue to plasma; k_3 and k_4 denote association and dissociation rate constants, respectively, between the free component and the specifically bound component.

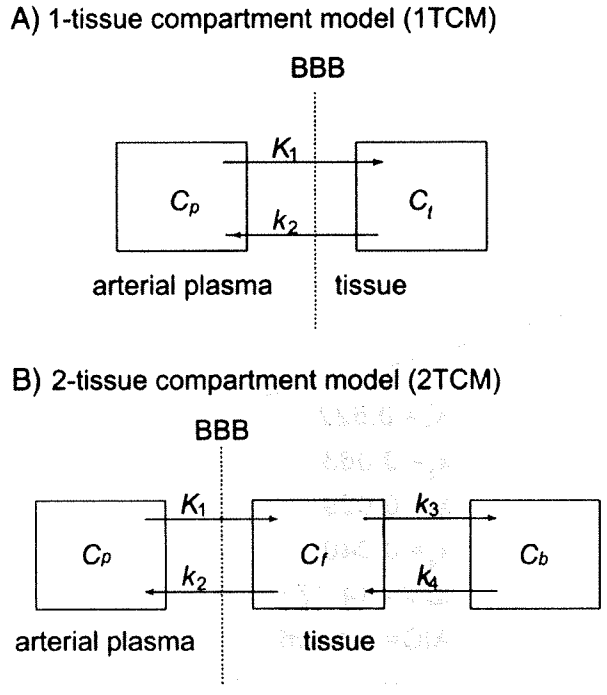

Fig. 2. The one-tissue compartment (1TCM) and two-tissue compartment (2TCM) models employed to analyze the kinetics of [^{11}C]donepezil.

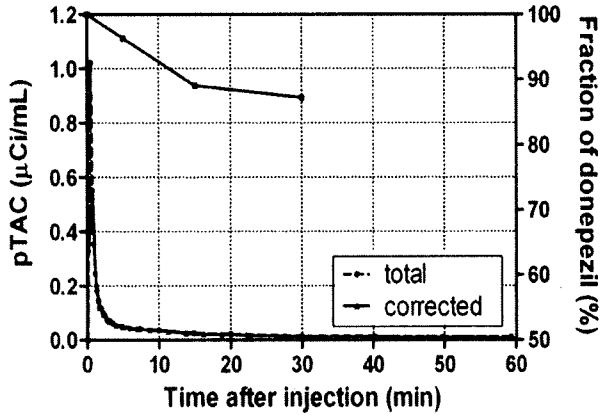

Fig. 3. Typical time–activity curve and the amount of intact [^{11}C]donepezil in arterial plasma. Total radioactivity and metabolite-corrected radioactivity are plotted in dashed and solid lines, respectively. The amount of intact [^{11}C]donepezil is shown in the upper curve. At 30 min, 87% of administered [^{11}C]donepezil remained in an intact form.

Calculations were performed using the dedicated software PMOD (PMOD Technologies) (Mikolajczyk et al., 1998). In the first step, a delay between tTACs and pTAC was estimated with the *k* parameters, as it was more sensitive than other parameters. In the second step, fixing the delay, all *k* parameters were estimated. Both steps were based on a nonlinear estimation (NLE) and were implemented using the Levenberg–Marquardt algorithm. Blood volumes were fixed at 3% (Martin et al., 1987). Initial values were 0.5 for K_1, 0.035 for k_2, 0.01 for k_3, and 0.01 for k_4. In this study, the convergences of estimates were confirmed by additional estimations, i.e., the initial values of the estimation were set to the estimated results of the second step. Goodness of fit was evaluated by χ^2 criterion. Model relevancy was assessed by Akaike's Information Criterion (AIC) (Akaike, 1974). The

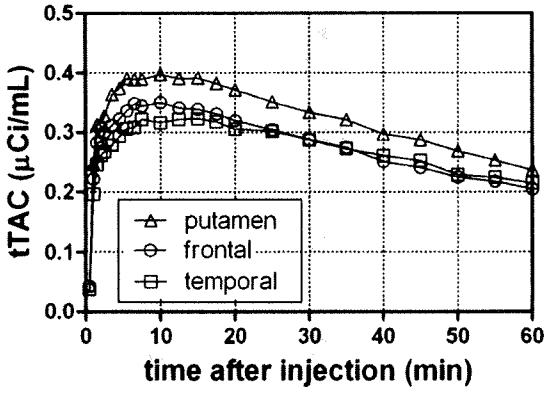

Fig. 4. Typical time–activity curves of the parietal cortex, frontal cortex, and putamen.

most appropriate model provides the smallest value of AIC. To evaluate kinetic parameter identifiability, standard error was calculated and the coefficient of variation of the parameter was shown as a percentage of parameter value (%COV). A distribution volume was calculated as K_1/k_2 in the 1TCM. The tDV was calculated as $(K_1/k_2)(1+k_3/k_4)$ in a 2TCM (Mintun et al., 1984). The tDVs with and without metabolite-corrected pTACs were compared with each other in order to investigate the possibility of omitting metabolite correction for pTAC.

In addition, Logan graphical analysis (Logan et al., 1990) was applied to the tTAC of each ROI and pTAC. The start time of the linear section in the graphical plot was fitted using an error criterion of 10%.

Results

pTACs and tTACs

pTACs with and without metabolite correction and time courses for the fraction of unchanged [^{11}C]donepezil in plasma are shown in Fig. 3. At 30 min post-injection, 91.0 ± 3.9% (mean ± SD) of administered [^{11}C]donepezil remained in the intact form. Plasma radioactivity peaked at 30–60 s post-injection, followed by a rapid decline. The plots in Fig. 4 describe typical tTACs in the parietal cortex, frontal cortex, and putamen. tTACs indicated initial rapid uptake of radioactivity followed by gradual clearance. A relatively high concentration

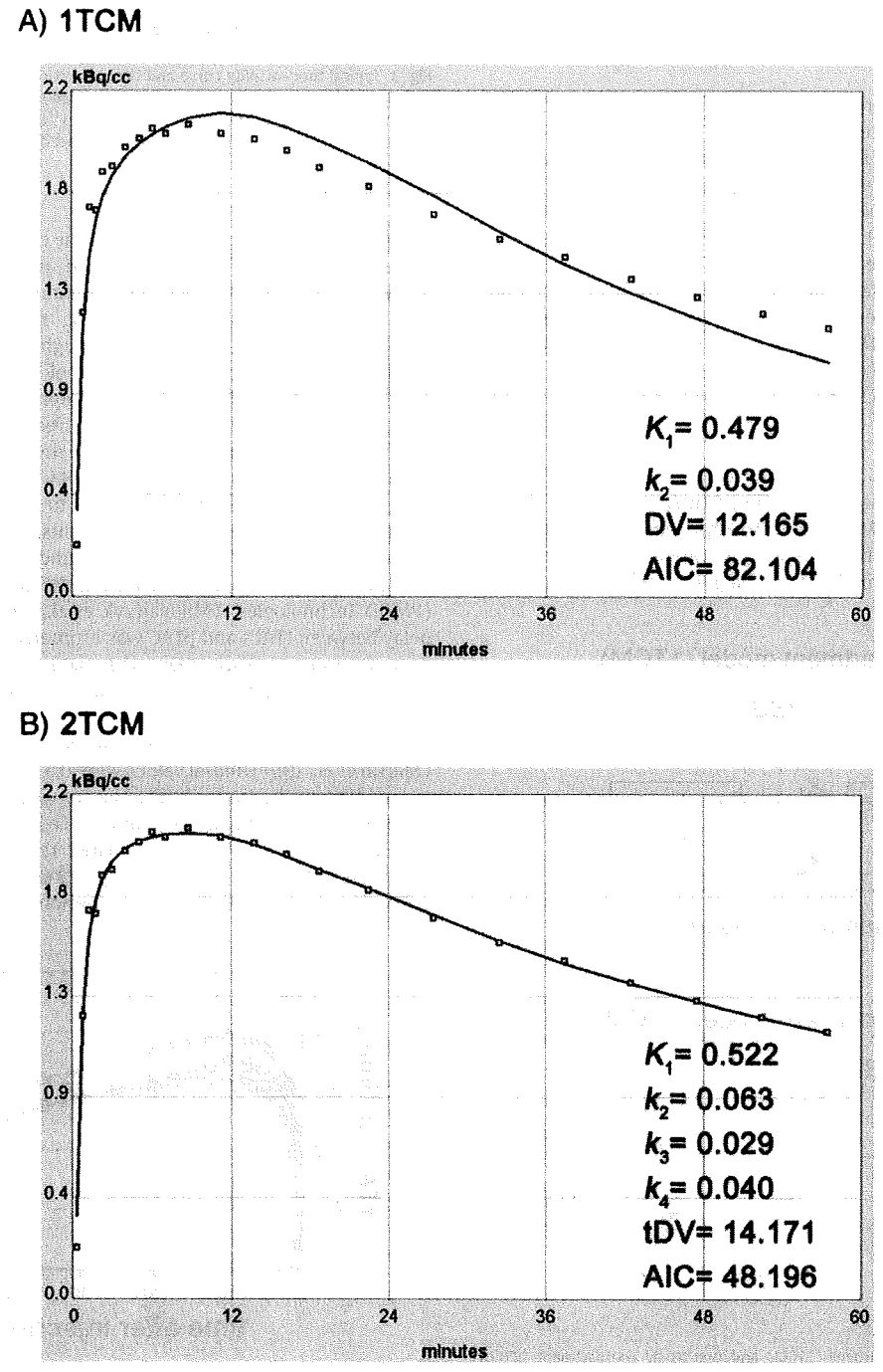

Fig. 5. Tissue time–activity curves (tTACs) of the occipital cortex and fit with the 1TCM and 2TCM. The dots (□) and the lines represent measured tTACs and model fits, respectively.

Table 1
Comparison of $\chi 2$ criterion and AIC of 1TCM and 2TCM.

	χ^2 criterion		AIC	
	1TCM	2TCM	1TCM	2TCM
Cerebellum	1.30 ± 0.40	0.30 ± 0.13	78.97 ± 7.69	46.30 ± 8.69
Putamen	1.62 ± 0.65	0.32 ± 0.09	83.42 ± 9.73	48.42 ± 7.19
Thalamus	1.90 ± 0.52	0.49 ± 0.28	87.95 ± 6.74	56.75 ± 11.61
Frontal	1.81 ± 0.64	0.38 ± 0.16	86.40 ± 8.67	51.07 ± 12.25
Temporal	1.24 ± 0.43	0.29 ± 0.07	77.60 ± 8.63	46.61 ± 5.90
Parietal	2.66 ± 0.74	0.46 ± 0.19	95.62 ± 7.56	55.66 ± 12.82
Occipital	1.58 ± 0.55	0.36 ± 0.18	83.27 ± 8.55	49.45 ± 12.66
Anterior cingulate	2.42 ± 0.95	0.44 ± 0.18	92.92 ± 8.84	55.01 ± 10.05
Posterior cingulate	2.54 ± 0.77	0.56 ± 0.34	94.50 ± 7.31	59.09 ± 13.59
Hippocampus	1.94 ± 0.63	0.53 ± 0.13	88.30 ± 7.47	60.38 ± 6.33

Mean ± SD in cerebral regions is shown.
AIC, Akaike's Information Criterion; 1TCM, one-tissue compartment model; 2TCM, two-tissue compartment model; SD, standard deviation.

of radioactivity of [^{11}C]donepezil was observed in the putamen, which is an AChE-rich region, whereas a moderate concentration was observed in the frontal and temporal cortices.

Kinetics

The results of curve-fitting by the 1TCM and 2TCM are superimposed in Fig. 5. There is considerable bias in the fit with a 1TCM, which, remarkably, is removed by a 2TCM. χ^2 criterion and AIC of two models are shown in Table 1. For both criteria, the values were lower for the 2TCM.

Estimated kinetic parameters in ten regions of the brain using the NLE algorithm are summarized in Table 2. The 1TCM parameters K_1 and k_2 were well identified in all regions, with %COV values close to 2% and 3%, respectively. The 2TCM kinetic parameters k_2, k_3, and k_4 were poorly identified in all regions, with %COV values close to 16%, 43%, and 32%, respectively. Finally, according to χ^2 criterion and AIC, a 2TCM was selected for further analysis.

The relationship between the mean tDV values in each cerebral region and post-mortem AChE values in human brain from the literature (Arai et al., 1984; Atack et al., 1986) is shown in Fig. 6. Post-mortem AChE values are expressed as ratios to the mean AChE value of cerebral cortices. The rank order of tDV values of cerebral regions (cerebral cortices < hippocampus < thalamus < cerebellum < putamen) was consistent with that of AChE activity.

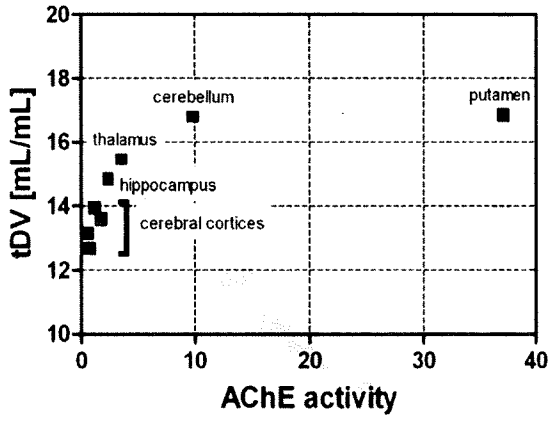

Fig. 6. Mean estimated total distribution volume (tDV) values of cerebral regions and post-mortem acetylcholinesterase (AChE) values in human brain obtained from the literature. Post-mortem AChE values are expressed as ratios to the mean AChE value of cerebral cortices.

In the estimation for validation of convergence, 95.0% of the estimates converged to within 5% of the results of the proposed two-step estimation, demonstrating the stability of the proposed estimation process.

Fig. 7 represents the influence of metabolite correction for pTAC on tDV. The values of tDVs with and without metabolite correction were well correlated ($y = 0.86x + 0.52$, $r^2 = 0.92$). The pTAC without metabolite correction caused an underestimation of 10.2% for the tDVs, and no regional or subject-oriented dependencies were found in the underestimation.

Table 2
Kinetic parameters (mean and %COV, $n = 6$) estimated by the 1TCM and the 2TCM.

	K_1 [mL/mL/min]		k_2 [L/min]		Distribution volume [mL/mL]	
	Mean	%COV	Mean	%COV	Mean	%COV
1TCM						
Cerebellum	0.52	1.89	0.03	3.70	14.94	2.56
Putamen	0.55	1.93	0.04	3.88	15.06	2.69
Thalamus	0.58	2.37	0.04	4.24	13.99	2.68
Frontal	0.48	1.98	0.04	3.82	11.83	2.57
Temporal	0.41	1.73	0.03	3.54	12.32	2.49
Parietal	0.50	2.80	0.04	4.72	11.17	3.05
Occipital	0.50	2.08	0.04	3.75	11.47	2.37
Anterior cingulate	0.47	2.37	0.04	4.63	11.85	3.34
Posterior cingulate	0.52	2.43	0.04	4.59	11.88	3.19
Hippocampus	0.38	2.41	0.03	5.00	12.50	3.58

	K_1 [mL/mL/min]		k_2 [L/min]		k_3 [L/min]		k_4 [L/min]		Total distribution volume [mL/mL]	
	Mean	%COV	Mean	%COV	Mean	%COV	Mean	%COV	Mean	%COV
2TCM										
Cerebellum	0.57	2.10	0.07	13.11	0.05	41.70	0.06	29.82	16.85	4.44
Putamen	0.62	2.99	0.08	15.54	0.07	42.98	0.06	26.67	16.86	3.71
Thalamus	0.66	3.06	0.09	18.20	0.08	55.55	0.07	35.92	15.50	4.66
Frontal	0.54	3.84	0.08	16.87	0.08	38.20	0.06	31.96	13.60	5.67
Temporal	0.45	3.54	0.06	15.21	0.06	41.85	0.05	29.60	13.96	4.53
Parietal	0.58	2.51	0.10	12.25	0.07	34.19	0.06	21.64	12.70	3.63
Occipital	0.54	1.93	0.07	9.77	0.04	46.72	0.05	48.23	13.18	7.56
Anterior cingulate	0.55	4.40	0.12	18.25	0.13	33.90	0.07	17.23	13.25	2.86
Posterior cingulate	0.60	6.42	0.11	21.59	0.09	43.91	0.06	42.40	13.88	9.63
Hippocampus	0.44	4.41	0.09	22.19	0.10	45.99	0.05	33.95	14.85	7.82

%COV, coefficient of variation of the parameter shown as a percentage of parameter value; 1TCM, one-tissue compartment model; 2TCM, two-tissue compartment model.

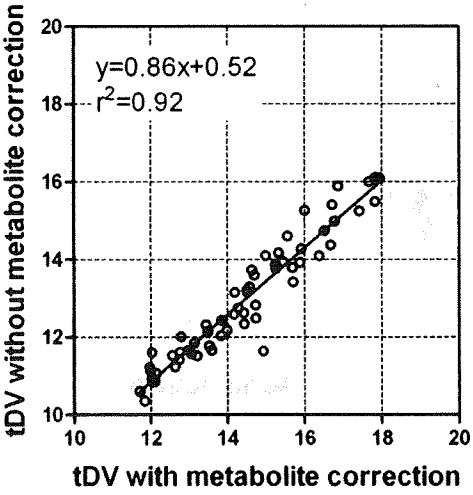

Fig. 7. Estimation of total distribution volumes (tDVs) (measured in mL/mL) with and without metabolite correction by the two-tissue compartment model (2TCM). All regions of interest (ROIs) obtained from each subject are plotted.

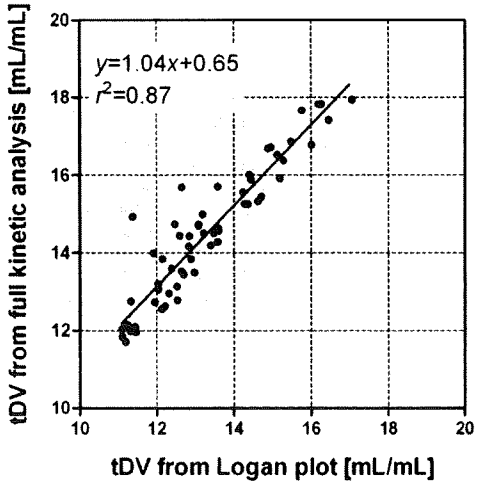

Fig. 9. Total distribution volumes estimated by the two-tissue compartment model (2TCM) were compared with those estimated by Logan graphical analysis. All regions of interest (ROIs) obtained from all subjects are plotted.

Logan plot analysis

Typical Logan plots are shown in Fig. 8. The start time of the linear section in the graphical plot was fitted using an error criterion of 10%, and good linear relationships were observed in the plots.

A comparison between the tDVs estimated by the 2TCM and those estimated by Logan plot analysis is shown in Fig. 9. The data obtained from all regions of all scans have been plotted. Both estimates were well correlated ($y = 1.04x + 0.65$, $r^2 = 0.87$), although Logan graphical analysis provided slightly lower tDV values than those of the 2TCM.

Images of tDV calculated by Logan graphical analysis are shown in Fig. 10. The tDV values were larger in the thalamus, basal ganglia, and cerebellar hemispheres, and smaller in the cortices.

Discussion

The study contrasted several methods for the kinetic analysis of [^{11}C]donepezil. Initially, compartment analysis of [^{11}C]donepezil in the brain was investigated. Theoretically, four parameters should be estimated in a 1TCM (K_1, k_2, delay, and blood volume) and six parameters should be estimated in a 2TCM (K_1, k_2, k_3, k_4, delay, and blood volume). As an estimation algorithm suffers from instability and dependency on the initial values, it is not feasible to estimate all the parameters simultaneously. Therefore, in order to reduce model specification, we fixed the blood volume at 3% in all brain regions, which is physiologically reasonable (Martin et al., 1987). In this study, the delay between tTAC and pTAC was estimated and fixed initially to reduce the number of parameters. The estimation of delay is more sensitive than k parameters, and converges more quickly than the other parameters. Practically, three parameters (K_1, k_2, and delay) for the 1TCM and five parameters (K_1, k_2, k_3, k_4, and delay) for the 2TCM were estimated simultaneously in the first step of the estimation, and then the delay estimate was used as a fixed parameter in the subsequent iteration of the fitting in the fixed parameters of the second step. Only two k parameters for the 1TCM and four k parameters for the 2TCM were estimated in the second step. The result of curve-fitting by the 2TCM was more accurate than that of the 1TCM, indicating that the state of equilibrium between free and bound tracer cannot be considered to be attained instantly. The values of the χ^2 criterion and AIC were lower for the 2TCM, which was therefore selected for further analysis. As individual identification of each parameter of the 2TCM was not reliable, and there were no usable reference regions for the [^{11}C]donepezil kinetic analysis, only the tDV was estimated (not each parameter or binding potential). Consequently, stable compartment analysis could be accomplished, and 94.3% of estimations could be considered reliable because they led to convergence within a 5% difference with the values of the first estimation.

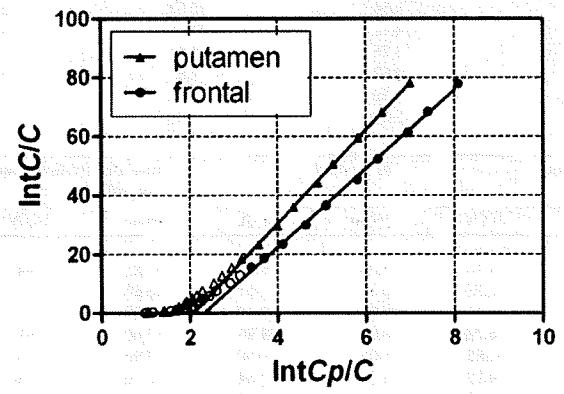

Fig. 8. Typical Logan plots. The plots for the frontal cortex and putamen are presented. C and C_p represent the measured time course of radioactivity in tissues and arterial plasma, respectively. The start time of the linear section in the graphical plot was fitted using an error criterion of 10%. Data used for the line estimation are shown as solid bullets.

Second, the compartment analysis was validated using Logan graphical analysis. Logan graphical analysis can estimate a stable tDV as it is free from the problems of initial values and misconvergency to a local minimum that occur with NLE. As shown in Fig. 8, linear relationships were established in Logan graphical analysis, demonstrating that it is indeed applicable to the analysis of [^{11}C]donepezil.

As shown in Fig. 9, the estimated tDVs from the kinetic analysis with the 2TCM and Logan plot analysis were well correlated, although Logan graphical analysis provided slightly lower tDV values than those of the 2TCM. The slight underestimation of tDV from Logan graphical analysis is probably due to the presence of statistical noise, as has been described previously (Logan, 2000). Logan graphical analysis offered stable estimates of tDV and gave more validity to the results of the kinetic analysis. The subsequent tDV images of the human brain (Fig. 10) showed a high density of [^{11}C]donepezil in the striatum, thalamus, and cerebellum, which are known to contain high densities of AChE compared with the cerebral cortex and hippocampus.

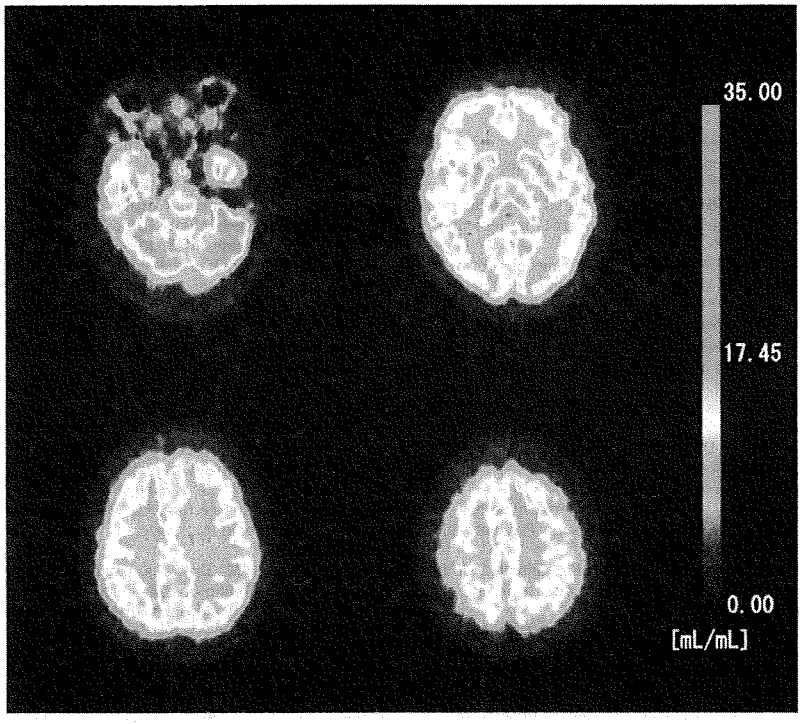

Fig. 10. Image of total distribution volumes (tDVs) derived with a Logan plot. tDV values were large in the thalamus, basal ganglia, and cerebellar hemispheres, and small in the cortices.

Regional tDVs of [^{11}C]donepezil correlated well, although not with perfect linearity, to regional AChE activity determined in human post-mortem studies (Arai et al., 1984; Atack et al., 1986), suggesting selective binding of donepezil to AChE. The lack of linear correspondence may be due to the fact that [^{11}C]donepezil uptake depends on regional blood flow rather than enzyme density in regions with high enzyme density such as the striatum and cerebellum, whereas tracer uptake is nearly proportional to enzyme activity in regions with moderate enzyme density such as the thalamus, hippocampus, and cerebral cortices. In addition, this lack of linearity might be attributable to limited spatial resolution of the PET camera. The tDV for a small region such as the putamen could be underestimated due to a partial volume effect of PET.

In this study, we did not conduct blocking trials. However, in a previous study involving rats (Funaki et al., 2003), a large amount of unlabeled donepezil (5 mg/kg) administered intraperitoneally reduced the striatum-to-cortex and brainstem-to-cortex ratios of [^{11}C]donepezil binding from 1.4 and 1.5 to 1.0 and 1.1, respectively. Moreover, in a study of patients with AD (Okamura et al., 2008), the available binding sites of [^{11}C]donepezil in the brain were partially blocked by orally administered donepezil (5 mg/day). An approximately 60% reduction of [^{11}C]donepezil binding was observed in the brain after oral administration at a therapeutic (single) dose. These results also confirm the validity of this method.

The possibility of omitting metabolite correction for the plasma input function was investigated in this study. As shown in Fig. 3, the intact form of [^{11}C]donepezil accounted for about 90% of the radioactivity in arterial plasma over 30 min, suggesting that peripheral metabolism of [^{11}C]donepezil is slow. The tDV values without metabolite correction were 10.3% lower than those with metabolite correction; however, tDV values with and without metabolite correction showed an almost identical relationship in all subjects and all ROIs. These results suggest that it is reasonable to omit metabolite correction.

Two lipophilic acetylcholine analogs, N-[^{11}C]methylpiperidin-4-yl acetate ([^{11}C]MP4A) and N-[^{11}C]methylpiperidin-4-yl propionate ([^{11}C]PMP), have been used with PET for AChE imaging (Iyo et al., 1997; Kuhl et al., 1999; Namba et al., 1999). Unlike [^{11}C]donepezil, these compounds are not reversible ligands, but are substrates for AChE, comparable to ^{11}C-L-deprenyl for the assay of monoamine oxidase B activity (Lammertsma et al., 1991). Their trapping in brain occurs as a function of their rates of conversion to less-diffusible metabolites. [^{11}C]MP4A and [^{11}C]PMP measure activities of AChE, while the distribution of [^{11}C]donepezil represents densities of AChE in each region of the brain. As the catalytic activity of AChE might not be well correlated with the density of AChE, the data from [^{11}C]MP4A, [^{11}C]PMP, and [^{11}C]donepezil should not generally yield nearly equivalent results. If AChE activities are functionally impaired or saturated, the results might be different.

In conclusion, our proposed method using the 2TCM is appropriate to provide tDV values for the kinetic analysis of [^{11}C]donepezil in human brain. The tDV correlated well with that derived from Logan graphical analysis, whose images enable visualization of the spatial distribution of AChE. Comparison of tDVs calculated with and without metabolite correction for plasma time–activity curves indicated that metabolite correction could be omitted.

This method enables quantitative analysis of AChE in the human brain, which is useful in various situations for patients with dementia. [^{11}C]donepezil-PET study can be exploited not only for the assessment of cholinergic dysfunction in patients, but also for the prediction of efficacy of treatment with AChE inhibitors. Moreover, by performing PET scans before and after treatment with AChE inhibitor, the AChE binding occupancy of orally administered AChE inhibitor can be measured, which facilitates the determination of clinical doses of AChE inhibitor.

Acknowledgments

This work was supported by Grants-in-Aid for Scientific Research from the Japan Society for the Promotion of Science (JSPS) and from the Ministry of Health, as well as by a grant for 'Molecular Imaging'

projects from the Ministry of Education, Culture, Sports, Science and Technology in Japan.

References

Akaike, H., 1974. A new look at the statistical model identification. IEEE Trans. Automat. Contr. AC19, 716–723.

Arai, H., Kosaka, K., Muramoto, O., Iizuka, R., 1984. [A biochemical study of cholinergic neurons of post-mortem brains from patients with Alzheimer-type dementia]. Rinsho Shinkeigaku 24, 1128–1135.

Atack, J.R., Perry, E.K., Bonham, J.R., Candy, J.M., Perry, R.H., 1986. Molecular forms of acetylcholinesterase and butyrylcholinesterase in the aged human central nervous system. J. Neurochem. 47, 263–277.

Blomqvist, G., Tavitian, B., Pappata, S., Crouzel, C., Jobert, A., Doignon, I., Di Giamberardino, L., 2001. Quantitative measurement of cerebral acetylcholinesterase using [^{11}C]physostigmine and positron emission tomography. J. Cereb. Blood Flow Metab. 21, 114–131.

Davies, P., Maloney, A.J., 1976. Selective loss of central cholinergic neurons in Alzheimer's disease. Lancet 2, 1403.

De Vos, F., Santens, P., Vermeirsch, H., Dewolf, I., Dumont, F., Slegers, G., Dierckx, R.A., De Reuck, J., 2000. Pharmacological evaluation of [11C]donepezil as a tracer for visualization of acetylcholinesterase by PET. Nucl. Med. Biol. 27, 745–747.

Francis, P.T., Palmer, A.M., Snape, M., Wilcock, G.K., 1999. The cholinergic hypothesis of Alzheimer's disease: a review of progress. J. Neurol. Neurosurg. Psychiatry 66, 137–147.

Frey, K.A., Koeppe, R.A., Kilbourn, M.R., Vander Borght, T.M., Albin, R.L., Gilman, S., Kuhl, D.E., 1996. Presynaptic monoaminergic vesicles in Parkinson's disease and normal aging. Ann. Neurol. 40, 873–884.

Fujiwara, T., Watanuki, S., Yamamoto, S., Miyake, M., Seo, S., Itoh, M., Ishii, K., Orihara, H., Fukuda, H., Satoh, T., Kitamura, K., Tanaka, K., Takahashi, S., 1997. Performance evaluation of a large axial field-of-view PET scanner: SET-2400W. Ann. Nucl. Med. 11, 307–313.

Funaki, Y., Kato, M., Iwata, R., Sakurai, E., Sakurai, E., Tashiro, M., Ido, T., Yanai, K., 2003. Evaluation of the binding characteristics of [5-(11)C-*methoxy*]donepezil in the rat brain for in vivo visualization of acetylcholinesterase. J. Pharmacol. Sci. 91, 105–112.

Iyo, M., Namba, H., Fukushi, K., Shinotoh, H., Nagatsuka, S., Suhara, T., Sudo, Y., Suzuki, K., Irie, T., 1997. Measurement of acetylcholinesterase by positron emission tomography in the brains of healthy controls and patients with Alzheimer's disease. Lancet 349, 1805–1809.

Koeppe, R.A., Holthoff, V.A., Frey, K.A., Kilbourn, M.R., Kuhl, D.E., 1991. Compartmental analysis of [11C]flumazenil kinetics for the estimation of ligand transport rate and receptor distribution using positron emission tomography. J. Cereb. Blood Flow Metab. 11, 735–744.

Kuhl, D.E., Koeppe, R.A., Minoshima, S., Snyder, S.E., Ficaro, E.P., Foster, N.L., Frey, K.A., Kilbourn, M.R., 1999. In vivo mapping of cerebral acetylcholinesterase activity in aging and Alzheimer's disease. Neurology 52, 691–699.

Lammertsma, A.A., Bench, C.J., Price, G.W., Cremer, J.E., Luthra, S.K., Turton, D., Wood, N.D., Frackowiak, R.S., 1991. Measurement of cerebral monoamine oxidase B activity using L-[11C]deprenyl and dynamic positron emission tomography. J. Cereb. Blood Flow Metab. 11, 545–556.

Logan, J., 2000. Graphical analysis of PET data applied to reversible and irreversible tracers. Nucl. Med. Biol. 27, 661–670.

Logan, J., Fowler, J.S., Volkow, N.D., Wolf, A.P., Dewey, S.L., Schlyer, D.J., MacGregor, R.R., Hitzemann, R., Bendriem, B., Gatley, S.J., et al., 1990. Graphical analysis of reversible radioligand binding from time–activity measurements applied to [N-11C-methyl]-(-)-cocaine PET studies in human subjects. J. Cereb. Blood Flow Metab. 10, 740–747.

Martin, W.R., Powers, W.J., Raichle, M.E., 1987. Cerebral blood volume measured with inhaled C15O and positron emission tomography. J. Cereb. Blood Flow Metab. 7, 421–426.

Mikolajczyk, K., Szabatin, M., Rudnicki, P., Grodzki, M., Burger, C., 1998. A JAVA environment for medical image data analysis: initial application for brain PET quantitation. Med. Inform. (Lond) 23, 207–214.

Mintun, M.A., Raichle, M.E., Kilbourn, M.R., Wooten, G.F., Welch, M.J., 1984. A quantitative model for the in vivo assessment of drug binding sites with positron emission tomography. Ann. Neurol. 15, 217–227.

Namba, H., Iyo, M., Fukushi, K., Shinotoh, H., Nagatsuka, S., Suhara, T., Sudo, Y., Suzuki, K., Irie, T., 1999. Human cerebral acetylcholinesterase activity measured with positron emission tomography: procedure, normal values and effect of age. Eur J. Nucl. Med. 26, 135–143.

Nelder, J.A., Mead, R., 1965. A simplex method for function minimization. Comput. J. 7, 308–313.

Okamura, N., Funaki, Y., Tashiro, M., Kato, M., Ishikawa, Y., Maruyama, M., Ishikawa, H., Meguro, K., Iwata, R., Yanai, K., 2008. In vivo visualization of donepezil binding in the brain of patients with Alzheimer's disease. Br. J. Clin. Pharmacol. 65, 472–479.

Parsey, R.V., Kegeles, L.S., Hwang, D.R., Simpson, N., Abi-Dargham, A., Mawlawi, O., Slifstein, M., Van Heertum, R.L., Mann, J.J., Laruelle, M., 2000. In vivo quantification of brain serotonin transporters in humans using [11C]McN 5652. J. Nucl. Med. 41, 1465–1477.

Perry, E.K., Curtis, M., Dick, D.J., Candy, J.M., Atack, J.R., Bloxham, C.A., Blessed, G., Fairbairn, A., Tomlinson, B.E., Perry, R.H., 1985. Cholinergic correlates of cognitive impairment in Parkinson's disease: comparisons with Alzheimer's disease. J. Neurol. Neurosurg. Psychiatry 48, 413–421.

Perry, E.K., Tomlinson, B.E., Blessed, G., Bergmann, K., Gibson, P.H., Perry, R.H., 1978. Correlation of cholinergic abnormalities with senile plaques and mental test scores in senile dementia. Br. Med. J. 2, 1457–1459.

Perry, E., Walker, M., Grace, J., Perry, R., 1999. Acetylcholine in mind: a neurotransmitter correlate of consciousness? Trends Neurosci. 22, 273–280.

Rogers, S.L., Farlow, M.R., Doody, R.S., Mohs, R., Friedhoff, L.T., 1998. A 24-week, double-blind, placebo-controlled trial of donepezil in patients with Alzheimer's disease. Donepezil Study Group. Neurology 50, 136–145.

Sakata, M., Kimura, Y., Naganawa, M., Oda, K., Ishii, K., Chihara, K., Ishiwata, K., 2007. Mapping of human cerebral sigma1 receptors using positron emission tomography and [11C]SA4503. Neuroimage 35, 1–8.

Tavitian, B., Pappata, S., Bonnot-Lours, S., Prenant, C., Jobert, A., Crouzel, C., Di Giamberardino, L., 1993. Positron emission tomography study of [11C]methyl-tetrahydroaminoacridine (methyl-tacrine) in baboon brain. Eur. J. Pharmacol. 236, 229–238.

Watabe, H., Channing, M.A., Der, M.G., Adams, H.R., Jagoda, E., Herscovitch, P., Eckelman, W.C., Carson, R.E., 2000. Kinetic analysis of the 5-HT2A ligand [11C]MDL 100,907. J. Cereb. Blood Flow Metab. 20, 899–909.

Whitehouse, P.J., Price, D.L., Struble, R.G., Clark, A.W., Coyle, J.T., Delon, M.R., 1982. Alzheimer's disease and senile dementia: loss of neurons in the basal forebrain. Science 215, 1237–1239.

Whitehouse, P.J., Hedreen, J.C., White III, C.L., Price, D.L., 1983. Basal forebrain neurons in the dementia of Parkinson disease. Ann. Neurol. 13, 243–248.

International Psychogeriatrics (2009), 21:1, 148–156 © 2008 International Psychogeriatric Association
doi:10.1017/S1041610208008132 Printed in the United Kingdom

Decreased cortical glucose metabolism in converters from CDR 0.5 to Alzheimer's disease in a community: the Osaki-Tajiri Project

Hiroshi Ishii,[1,2] Hiroyasu Ishikawa,[1,3] Kenichi Meguro,[1,3] Manabu Tashiro[4] and Satoshi Yamaguchi[1,3]

[1] *Department of Geriatric Behavioral Neurology, Tohoku University Graduate School of Medicine, Sendai, Japan*
[2] *Kawasaki Kokoro Hospital, Kawasaki, Japan*
[3] *The Osaki-Tajiri SKIP Center, Osaki, Japan*
[4] *Division of Nuclear Medicine, Cyclotron Radioisotope Center, Tohoku University, Sendai, Japan*

ABSTRACT

Background: Several follow-up [^{18}F]fluorodeoxy glucose (FDG)-positron emission tomography (PET) studies have been performed in patients with mild cognitive impairment, but none have examined subjects with a Clinical Dementia Rating (CDR) of 0.5. Therefore, we used FDG-PET to investigate whether baseline glucose metabolism (CMRglc) in CDR 0.5 converters to dementia showed changes consistent with early Alzheimer's disease (AD).

Methods: Based on our earlier study, which we refer to as Prevalence Study 1998, we were able to examine 14 CDR 0, 42 CDR 0.5, and 12 AD subjects with PET and follow these subjects for five years. Baseline neuropsychological and CMRglc values were compared among groups of CDR 0, CDR 0.5/converters, CDR 0.5/non-converters, and AD subjects.

Results: All CDR 0 subjects were reassessed as CDR 0 after the five-year period. For CDR 0.5 subjects, 20 had converted to AD and 22 remained as CDR 0.5. In cognitive tests, CDR 0.5/converters showed significantly deteriorated recent memory function compared with CDR 0.5/non-converters at the baseline evaluation. Most brain areas showed decreased CMRglc in AD patients. CDR 0.5/converters had a significantly lower baseline CMRglc in the right cingulate, left inferior parietal and left temporal gyrus compared with CDR 0.5/non-converters.

Conclusions: Our findings suggest that CDR 0.5/converters have a baseline metabolic decline in areas that might be specific to AD.

Key words: MCI, CDR 0.5, FDG, PET, Alzheimer's disease

Introduction

Early diagnosis of the borderline condition between healthy aging and dementia may be important for health policy planning for dementia prevention or early intervention, since some borderline cases are reported to be reversible (Larrieu *et al.*, 2002). This condition is referred to as mild cognitive impairment (MCI) (Petersen *et al.*, 1997) or Clinical Dementia Rating (CDR; Morris, 1993) 0.5, and the rate of progression to dementia is 8–20% per year. Impairment of cognitive functions such as recent memory and executive function (Chen *et al.*, 2000) and a lower clinical observation score (Morris *et al.*, 2001) are predictors of decline.

Hippocampal atrophy (Visser *et al.*, 2002) shown by magnetic resonance imaging (MRI) is characteristic of the neurological background of CDR 0.5 subjects, particularly in association with early Alzheimer's disease (AD). Five major longitudinal studies of MCI have been performed using the baseline cerebral metabolic rate for glucose (CMRglc) determined by positron emission tomography (PET) with [^{18}F]fluoro-deoxyglucose (FDG) (Arnaiz *et al.*, 2001; Chetelat *et al.*, 2003; Drzezga *et al.*, 2003; Mosconi *et al.*, 2004; Fellgiebel *et al.*, 2007). All these studies used clinic samples, with four using neuropsychological tests based on Petersen's MCI criteria (Petersen *et al.*, 1997) and the fifth using Global Deterioration Scale (GDS)

Correspondence should be addressed to: Kenichi Meguro, MD, PhD, Department of Geriatric Behavioral Neurology, Tohoku University Graduate School of Medicine, 2-1, Seiryo-machi, Aoba-ku, Sendai 980-8575, Japan. Email: k-meg@umin.ac.jp. Received 19 May 2008; revision requested 28 Jul 2008; revised version received 17 Sep 2008; accepted 25 Sep 2008. First published online 1 December 2008.

3 criteria (Reisberg *et al.*, 1982). After following the subjects for 1–3 years, amnestic MCI subjects showing AD-like metabolic changes (decreased CMRglc in the temporoparietal areas and posterior cingulate) were found to be at risk for conversion to AD.

Follow-up FDG-PET has not been performed in CDR 0.5 subjects, but follow-up with other approaches has indicated that CDR 0.5 subjects with a higher CDR-sum of boxes (SB) score more frequently decline to AD compared with those with lower CDR-SB scores (Morris *et al.*, 2001). CDR 0.5 subjects with a higher SB score also show decreased metabolism in AD-specific areas (Perneczky *et al.*, 2007). These results suggest that CDR 0.5 converters to AD have an AD-like metabolic pattern, and the aim of this study was to examine this hypothesis using FDG-PET in our MCI/CDR 0.5 cohort.

The Osaki-Tajiri Project, previously called the Tajiri Project, is a community-based program on stroke, dementia, and bed-confinement prevention in Osaki, northern Japan. In our Prevalence Study 1998 (Meguro *et al.*, 2002), we reported rates of CDR 0.5 and MCI of 30.1% and 4.9%, respectively, with CDR 0.5 having a significantly greater prevalence (Meguro *et al.*, 2004). Among the participants in Prevalence Study 1998, we were able to examine CMRglc for 68 people and follow them for five years, after which we examined the incidence of dementia that developed in CDR 0 and 0.5 subjects (Incidence Study 2003; Meguro *et al.*, 2007). In the current study, we investigated whether the baseline CMRglc of CDR 0.5 converters to dementia manifests as metabolic changes specific to early AD.

Methods

Participants

In Prevalence Study 1998, 564 adults from among an epidemiologic population of 1,654 were randomly selected to undergo MRI (1.5T, Shimazu, Japan). The cost of all the MRIs was officially borne by the town. Finally, 497 participants agreed to undergo MRI: 346 CDR 0 (healthy), 119 CDR 0.5 (questionable dementia), and 32 CDR 1+ (dementia) subjects. T1-weighted (TR/TE 400/14) and T2-weighted (TR/TE 3000/90) images were used for assessing atrophy and cerebrovascular diseases, as described previously (Meguro *et al.*, 2002).

Owing to the limited time available for FDG-PET examination at Tohoku University Cyclotron Radioisotope Center (an average of four patients a month), we had to select subjects who would receive PET. From the 497 subjects who underwent MRI, we randomly selected 35 CDR 0 (10% of 346) and 60 CDR 0.5 (50% of 119) subjects, and all 14 AD patients among the CDR 1+ group, for PET. Finally, we were able to examine 68 subjects using PET: 14 CDR 0, 42 CDR 0.5, and 12 AD. The other subjects refused to undergo PET examinations due to "psychological" reasons and the travelling distance between the community and the PET center (a one-hour drive).

All AD patients had a rating of CDR 1 and met the NINCDS-ADRDA criteria for probable AD (McKhann *et al.*, 1984). All CDR 0.5 subjects showed mild cognitive dysfunction, but this did not affect their daily lives in the community and none met the DSM-IV criteria for dementia (American Psychiatric Association, 1994). All 68 subjects met the following inclusion criteria: (1) no history of stroke, head injury or systemic disorders that could affect brain function, and normal values of vitamin B_1, B_6, B_{12}, folate, and thyroid hormones; (2) no cerebrovascular diseases as shown by MRI, and no marked neurological signs and symptoms; and (3) agreement of the subjects and family members to participate in Incidence Study 2003 and to be followed for five years.

Written informed consent was obtained from all CDR 0 and 0.5 subjects and from the families of CDR 0.5 and AD patients. The study was approved by the Ethical Committee of the Cyclotron Radioisotope Center of Tohoku University and the Tajiri SKIP Center.

CDR assessment

A clinical team of doctors and public health nurses determined the CDR while blinded to the cognitive tests (see below) and PET findings. Before being interviewed by the doctors, public health nurses visited the participants' homes to evaluate their daily activities. Observations by family members regarding the participants' lives were described in a semi-structured questionnaire; for participants who lived alone, public health nurses visited them frequently to evaluate their daily lives. The participants were interviewed by doctors to assess episodic memory, orientation, problem solving and judgment. Finally, the CDR stages were decided at a joint meeting, with reference to the information provided by the family. A reliable Japanese version of the CDR Work Sheet (Meguro, 2004) has been established, and one of the authors (K.M) has been certified as a CDR rater at the Alzheimer's Disease Research Center, Washington University School of Medicine. CDR 0.5 participants who converted to AD were classified as CDR 0.5/converters and those who did not convert as CDR 0.5/non-converters.

The CDR was evaluated using the same approach at baseline and follow-up.

Cognitive assessment

A team of trained psychologists performed cognitive tests while blinded to the CDR stages and PET findings. These tests included the Mini-mental State Examination (MMSE; Folstein *et al.*, 1975) and the Cognitive Abilities Screening Instrument (CASI) (Teng *et al.*, 1994). The CASI has nine domains: long-term memory, short-term memory, attention, concentration/mental manipulation, orientation, visual construction, abstraction and judgment, list-generating fluency, and language. The long-term memory domain evaluates knowledge and remote memory, and herein we refer to this domain as "remote memory." The short-term memory domain assesses delayed recall of three words presented orally and immediate recall of five objects presented visually, and we refer to this domain as "recent memory."

PET

The PET study was performed with a model PT931/04-12 scanner (CTI Inc., USA; axial/transaxial resolutions: 8 mm) using [^{18}F]fluoro-deoxyglucose (FDG) (Phelps *et al.*, 1979; Reivich *et al.*, 1979). A short cannula was placed in a radial artery for blood sampling. Each subject was positioned with the OM line parallel to the detector rings according to brain slices collected by MRI. A cross of light was projected onto marks on the subject's head, which were set at standard points of 30 mm and 77 mm above and parallel to the OM line. A 20-minute transmission scan was performed using a ^{68}Ge/^{68}Ga external ring source. Thirty to 45 minutes after injection of 5–12 mCi of FDG, two emission scans were performed and data were collected simultaneously from each of seven contiguous axial sections. A total of 14 slices parallel to the OM line with a thickness of 6 mm were analyzed, encompassing virtually the whole brain. The detailed methodology has been described previously (Yamaguchi *et al.*, 1997).

Imaging analyses

ROI

After two different pairs of axial T1-weighted MRI and PET images were matched with each other at the same brain slice, the position of the regions of interest (circular ROIs, 2.7 cm^2) were defined manually using the overlapped images. A total of 13 ROIs in each hemisphere were selected: upper frontal, anterior frontal, inferior frontal, parietal, temporo-parieto-occipital, primary auditory, temporal, hippocampus, primary visual, occipital, basal ganglia, cerebellum, and white matter. The detailed methodology has been described previously (Yamaguchi *et al.*, 1997).

SPM

Basic image processing and voxel-based data analysis were performed using SPM2 (Wellcome Department of Cognitive Neurology, London, U.K.) on a Windows XP machine. PET data were subjected to an affine and non-linear spatial normalization into the standard MNI PET template of SPM2, and to re-slicing of 2×2×2 mm. The PET images were smoothed using an isotropic Gaussian filter of 12 mm in diameter to compensate for intersubject gyral variability and to reduce high-frequency noise. The anatomically standardized images were then normalized by ANCOVA to a mean value of 50 mg/100 g/min. The four groups (CDR 0, CDR 0.5/non-converters, CDR 0.5/converters, AD) were compared with ANCOVA (covariance of age and educational level). Pairs of groups were compared with unpaired t-tests. For multiple comparison, significance was accepted if the voxels survived an uncorrected threshold of $p<0.001$.

Individual analysis

Individual CMRglc pattern analysis was conducted using the classification of Silverman *et al.* (2001): N1, normal metabolism; N2, global hypometabolism; N3, focal hypometabolism; P1, parietal/temporal with/without frontal hypometabolism; P2, frontal predominant hypometabolism; P3, hypometabolism of both the caudate head and lentiform nuclei. N indicates non-progressive PET patterns, and P shows progressive PET patterns. P1 indicates a PET pattern consistent with AD, and P2 and P3 indicate progressive but non-AD patterns. The patterns were compared between CDR 0.5/non-converters and CDR 0.5/converters by χ^2 test.

Clinical reassessments

In Incidence Study 2003, the CDR stages of all the subjects in the current PET study were reassessed to determine whether they met the criteria for dementia and AD. The reassessments were performed by evaluators who were blinded to the baseline CDR, neuropsychological tests, and PET findings. We mainly focused on CDR 0.5 subjects to determine whether they met the criteria for CDR 1 and AD.

Results

Clinical outcome

All participants in the CDR 0 group were reassessed as CDR 0 after the five-year period. In the CDR 0.5 group, 20 participants converted to AD (CDR 0.5/converters) and 22 participants remained as CDR 0.5 (CDR 0.5/non-converters). All AD patients declined to CDR 2. The demographics of the four groups are shown in Table 1. Age and educational level did not differ significantly among the groups. The AD group had significantly lower cognitive scores compared with the other groups.

Cognitive impairment

The CASI scores of the four groups are shown in Table 2. The AD group had significantly lower scores for all domains except "remote memory," compared with the other groups. CDR 0.5/converters showed a significantly lower "recent memory" score compared with CDR 0.5/non-converters.

Baseline glucose metabolism

Absolute rCMRglc values were calculated using arterial blood sampling and autoradiography. Using the ROI method, we found that the AD group had severely decreased rCMRglc compared with other groups, except in the basal ganglia and white matter, as shown in Table 3. There was no significant difference between CDR 0.5/non-converters and the CDR 0 group. However, CDR 0.5/converters had decreased rCMRglc in the temporoparieto-occipital (TPO) and hippocampus compared with CDR 0 subjects, and decreased rCMRglc in the TPO compared with CDR 0.5/non-converters.

SPM

Comparisons of CDR 0.5 subjects with CDR 0 subjects and AD patients

Comparisons of CDR 0.5/converters and CDR 0.5/non-converters with CDR 0 subjects are shown in Figure 1, and similar comparisons with AD

Table 1. Demographics of the study population at baseline

GROUP	MALE/FEMALE	AGE (y)	EDUCATION (y)	CASI TOTAL
CDR 0	4/10	77.7 (1.5)	8.4 (0.2)	89.7 (1.4)
CDR 0.5/non-converters	7/15	78.0 (1.6)	8.4 (0.2)	87.9 (1.6)
CDR 0.5/converters	7/13	78.4 (1.7)	9.1 (0.3)	79.9 (1.7)
AD	6/6	80.0 (1.8)	8.3 (0.4)	50.7 (2.4)†

Shown are the mean (SD).
Age (one-way ANOVA, F = 2.410, p = 0.081) and educational level (F = 0.393, p = 0.0759) did not differ significantly among the groups. The AD group had significantly lower cognitive scores compared with the other groups (F = 35.810, p<0.0001)(†).
CDR = Clinical Dementia Rating, AD = Alzheimer's disease.
CASI = Cognitive Abilities Screening Instrument.

Table 2. Cognitive performances of four groups at baseline

CASI ITEMS	CDR 0	CDR 0.5/ NON-CONVERTERS	CDR 0.5/ CONVERTERS	AD	F VALUE	p VALUE
Remote Memory	10.0 (0.0)	10.0 (0.0)	9.6 (0.8)	8.3 (2.9)	2.209	0.073
Recent Memory	10.8 (1.6)	10.8 (1.6)	6.8 (3.1)[a,b]	2.8 (1.9)[a,b,c]	20.900	0.000
Attention	6.5 (1.3)	6.8 (1.7)	6.9 (1.0)	4.4 (2.0)[b,c]	3.860	0.006
Concentration/ Mental Manipulation	7.3 (1.7)	7.6 (1.6)	7.5 (2.0)	3.8 (3.4)[a,b,c]	6.402	0.000
Orientation	17.8 (0.4)	16.7 (3.1)	15.2 (3.3)	5.3 (3.7)[a,b,c]	26.056	0.000
Visual Construction	9.9 (0.3)	9.7 (0.7)	9.7 (0.5)	7.7 (2.4)[a,b,c]	5.880	0.000
Abstraction and Judgement	9.2 (2.2)	8.8 (2.1)	6.9 (2.0)	5.1 (2.9)[a,b]	5.886	0.000
List-generating Fluency	8.0 (1.8)	7.6 (2.2)	6.5 (1.8)	4.3 (2.0)[a,b]	6.159	0.000
Language	9.8 (0.4)	9.9 (0.3)	9.7 (0.5)	8.2 (2.0)[a,b]	4.057	0.005

Showns are the mean (SD).
ANCOVA among four groups with the age and education level as covariance was performed.
The AD group had significantly lower scores for all domains except "remote memory," compared with the other groups (ANCOVA, covariance of age and educational level, p = 0.008). CDR 0.5/converters showed a significantly lower "recent memory" score compared with CDR 0.5/non-converters (ANCOVA, covariance of age and educational level, p = 0.008). post hoc tests, significantly (p<0.05) different from Normal (a), CDR 0.5/non-converters (b), and CDR 0.5/converters (c).
CDR = Clinical Dementia Rating, AD = Alzheimer's disease.